We are IntechOpen, the world's leading publisher of Open Access books
Built by scientists, for scientists

6,900
Open access books available

185,000
International authors and editors

200M
Downloads

154
Countries delivered to

Our authors are among the

TOP 1%
most cited scientists

12.2%
Contributors from top 500 universities

CLARIVATE ANALYTICS
BOOK CITATION INDEX
INDEXED

WEB OF SCIENCE™

Selection of our books indexed in the Book Citation Index
in Web of Science™ Core Collection (BKCI)

Interested in publishing with us?
Contact book.department@intechopen.com

Numbers displayed above are based on latest data collected.
For more information visit www.intechopen.com

Chapter

Robust and Adaptive Control for Synchronous Generator's Operation Improvement

Jožef Ritonja

Abstract

Synchronous generators produce almost 95% of the world's electricity. Even a small improvement in their efficiency represents huge savings. Electromechanical oscillations of synchronous generators are harmful—they cause losses and can even lead to instability. An additional control system, called a power system stabilizer (PSS), is used to damp the oscillations of synchronous generators. The commercial realizations of the power system stabilizers are based on the use of the linear control theory. The effectiveness of these power system stabilizers is small, because of the nonlinear and time-varying characteristics of the synchronous generators. The application of robust and adaptive control represents an adequate theoretical basis for ensuring optimal damping of the electromechanical oscillations in a wide operating range. This work reviews the applicability of the advanced control theories to develop power system stabilizers. The work is focused on selecting the appropriate robust and adaptive control theories for the power system stabilizer implementation. The applicability and advantages are presented of the sliding mode control and the direct adaptive control, along with an evaluation of their impact on the operation improvement.

Keywords: sliding mode control, direct adaptive control, synchronous generator, power system stabilizer, operation of synchronous generator

1. Introduction

Synchronous generators are the most important electrical machines. They produce the majority of the world's electricity. In 2017, global electricity production was 25,721 TWh [1]. Assuming that the share of solar thermal sources is negligible compared to the share of solar photovoltaic sources, it can be estimated that about 98.2% of the total global energy is produced by electric generators. After analyzing the data, it can be estimated that synchronous generators produce 93.8% of the world's electricity and induction generators 4.4% of the total production of the world's electricity. The estimate is based on data for 2017. These, and also the following data, are obtained from statistics reports of the International Energy Agency [1].

An additional important point is that electricity trading and, thus, long-distance transmission of electricity are increasing significantly. In 2017, OECD countries produced 11,051 TWh of electricity, with a trading volume of 408 TWh,

representing 3.7% of total production. Even more interesting is the growth rate of electricity trade. In the OECD, imports of electricity grew from 89 TWh in 1974 to 480 TWh in 2018, representing an average annual growth rate of 4.0%, compared to 2.1% growth in overall electricity supply.

The facts that the majority of the world's electricity is produced by synchronous generators and that a large amount of the world's electricity is transmitted over long distances result in significant oscillations of the produced and transmitted power. Despite the relatively small oscillations—the ratio of the amplitude of the oscillations of the transmitted power relative to the mean value of the transmitted power is mainly smaller than 10%—the total global losses due to the extremely large volume of production and transmission of electricity are not negligible. In terms of saving energy, it makes sense to reduce these losses.

The amount of the transmitted power oscillations can be affected by optimizing the topology of the new networks, by reconfiguring of the existing networks, by selection of the better damped new synchronous generators, and by replacement of the existing synchronous generators with the better damped ones. These solutions are expensive, and their realization also depends on other social and ecological factors. Therefore, it is a much more suitable solution to use a control system to damp the power system oscillations. In power systems, control systems called power system stabilizers (PSS) are used to suppress oscillations. PSS represent the best and the most economical solution for damping of the power systems' oscillations. PSS are simple to realize—they are mainly a part of the controller of the synchronous generator's static semiconductor excitation system. PSS, based on information of the oscillations of the transmitted power, rotor speed, rotor angle, or rotor acceleration, generate an additional reference signal for the rotor current control system. This additional reference signal represents the supplementary input to the static semiconductor excitation system, which is connected to rotor field winding.

Conventional PSS design is based on a linear control theory. Conventional PSS is simple to realize, but its application shows nonoptimal damping through the entire operating range; by varying the operating point, the synchronous generator's dynamic characteristics also vary; the fact is that PSS, which was determined for the nominal operating point, does not assure optimal damping in the entire operating range. Such a PSS reduces transmission losses optimally only at the operating point for which the PSS parameters are selected. Due to the large changes in the transmitted power and the large variations in power generation of the synchronous generators, conventional PSS are not satisfactory for use in modern power systems. To improve PSS performance, major modern control theories have been tested in the past decade for the purposes of PSS design. Of all the methods, robust and adaptive control has been implemented to be the most suitable for the design of PSS. Both control methods have been used in order to assure optimal damping through the entire operating range of the synchronous generators. The use of adaptive control is possible because the loading variations and, consequently, the variations of the dynamic characteristics of the synchronous generators are, in most cases, substantially slower than the dynamics of the adaptation mechanism [2].

Reduction of losses is not the sole and basic task of PSS. Even more important is that the PSS improves the stability of the power system and allows the transfer of power from the synchronous generator to the power system or between different points in the power system as near as possible to the stability limit of the transmission. In the presented work, however, we show the results of our study, which will show the applicability of the developed robust and adaptive PSS, mainly for the improvement of the damping of the power system oscillations.

For a detailed analysis of the benefits of the advanced PSS, a mathematical model of the synchronous generator is necessary. In this work, we first present the mathematical model of the synchronous generator connected to the power system, which is convenient for analysis of the physical characteristics of the power system and is appropriate at the same time for the controller design and synthesis. We focus our work on the analysis of a system where a single synchronous generator is connected to an infinite bus. In Section 3, we attempt to estimate the amount and dynamics of the oscillations in the power systems. A thorough analysis is made and presented for the first time. The conventional PSS control system is presented in Section 4. By means of the derived mathematical model of the synchronous generator, we estimate the improvement of the power system damping due to implementation of the conventional PSS. From the analysis, it is evident that conventional PSS does not assure optimal damping in the entire operating range. Therefore, advanced control theories for PSS design and synthesis are presented in Sections 5 and 6. In Section 5, the robust control system theory is used for PSS design. The suitable direct adaptive control theory is presented in Section 6. The PSS control system developed on the basis of the presented theories and the results of the implementation of the advanced control theories for PSS design and synthesis are shown in Section 7.

2. Mathematical model of the synchronous generator connected to the power system

The seventh-order nonlinear model of the synchronous machine connected to the infinite bus is the most detailed mathematical model of the synchronous generator connected to the large power system with constant frequency and constant voltage (=infinite bus) through the transmission line [3]. Park's matrix transformation is used to transform the origin windings' equations into a model with orthogonal axes. On this basis, the magnetic coupling of the stator, field, and damper windings is represented as a function of the position of the machine's rotor. The seventh-order model is represented in the form of a nonlinear state-space model [4]. The model's inputs are mechanical torque $T_m(t)$ and rotor excitation winding voltage $E_{fd}(t)$. The model's state-space variables are stator d-axis flux linkage $\lambda_d(t)$, stator q-axis flux linkage $\lambda_q(t)$, rotor excitation winding flux linkage $\lambda_F(t)$, rotor d-axis damper winding flux linkage $\lambda_D(t)$, rotor q-axis damper winding flux linkage $\lambda_D(t)$, mechanical rotor speed $\omega(t)$, and electric rotor angle $\delta(t)$. The seventh-order model is described by sets of algebraic equations (Eqs. (1)–(10)) [5]:

$$\lambda_{AD}(t) = L_{MD}\left(\frac{\lambda_d(t)}{l_d} + \frac{\lambda_F(t)}{l_F} + \frac{\lambda_D(t)}{l_D}\right) \tag{1}$$

$$\lambda_{AQ}(t) = L_{MQ}\left(\frac{\lambda_q(t)}{l_q} + \frac{\lambda_Q(t)}{l_Q}\right) \tag{2}$$

$$i_d(t) = \frac{1}{l_d}(\lambda_d(t) - \lambda_{AD}(t)) \tag{3}$$

$$i_q(t) = \frac{1}{l_q}(\lambda_q(t) - \lambda_{AQ}(t)) \tag{4}$$

$$i_F(t) = \frac{1}{l_F}(\lambda_F(t) - \lambda_{AD}(t)) \tag{5}$$

$$i_{\mathrm{D}}(t) = \frac{1}{l_{\mathrm{D}}}\left(\lambda_{\mathrm{D}}(t) - \lambda_{\mathrm{AD}}(t)\right) \tag{6}$$

$$i_{\mathrm{Q}}(t) = \frac{1}{l_{\mathrm{Q}}}\left(\lambda_{\mathrm{Q}}(t) - \lambda_{\mathrm{AQ}}(t)\right) \tag{7}$$

$$v_{\mathrm{d}}(t) = -\sqrt{3}V_{\infty}\sin\left(\delta(t)\right) + R_{e}i_{\mathrm{d}}(t) + \omega(t)L_{e}i_{\mathrm{q}}(t) \tag{8}$$

$$v_{\mathrm{q}}(t) = \sqrt{3}V_{\infty}\cos\left(\delta(t)\right) + R_{e}i_{\mathrm{q}}(t) + \omega(t)L_{e}i_{\mathrm{d}}(t) \tag{9}$$

$$T_{\mathrm{e}}(t) = \frac{1}{3}\left(i_{\mathrm{q}}(t)\lambda_{\mathrm{d}}(t) - i_{\mathrm{d}}(t)\lambda_{\mathrm{q}}(t)\right) \tag{10}$$

and differential equations (Eqs. (11)–(17)):

$$\dot{\lambda}_{\mathrm{d}}(t) = \omega_{s}\left(-R_{s}i_{\mathrm{d}}(t) - \omega(t)\lambda_{\mathrm{q}}(t) - v_{\mathrm{d}}(t)\right) \tag{11}$$

$$\dot{\lambda}_{\mathrm{q}}(t) = \omega_{s}\left(-R_{s}i_{\mathrm{q}}(t) + \omega(t)\lambda_{\mathrm{d}}(t) - v_{\mathrm{q}}(t)\right) \tag{12}$$

$$\dot{\lambda}_{\mathrm{F}}(t) = \omega_{s}(-R_{\mathrm{F}}i_{\mathrm{F}}(t) + E_{\mathrm{fd}}(t)) \tag{13}$$

$$\dot{\lambda}_{\mathrm{D}}(t) = \omega_{s}(-R_{\mathrm{D}}i_{\mathrm{D}}(t)) \tag{14}$$

$$\dot{\lambda}_{\mathrm{Q}}(t) = \omega_{s}\left(-R_{\mathrm{Q}}i_{\mathrm{Q}}(t)\right) \tag{15}$$

$$\dot{\omega}(t) = \frac{1}{2H}\left(T_{\mathrm{m}}(t) - T_{\mathrm{e}}(t)\right) \tag{16}$$

$$\dot{\delta}(t) = \omega_{s}(\omega(t) - 1) \tag{17}$$

where $i_{\mathrm{d}}(t)$ and $i_{\mathrm{q}}(t)$ are stator d- and q-axis currents [pu]; $i_{\mathrm{F}}(t)$ is field current [pu]; $i_{\mathrm{D}}(t)$ and $i_{\mathrm{Q}}(t)$ are damping d- and q-axis currents [pu]; $v_{\mathrm{d}}(t)$ and $v_{\mathrm{q}}(t)$ are stator terminal d- and q-axis voltages [pu]; $\lambda_{\mathrm{AD}}(t)$ and $\lambda_{\mathrm{AQ}}(t)$ are d- and q-axis mutual flux linkages [pu]; R_{e} and L_{e} are transmission line resistance and reactance [pu]; V_{∞} is infinite bus voltage [pu]; $T_{\mathrm{e}}(t)$ is electromagnetic torque [pu]; L_{MD}, L_{MQ}, L_{AD}, and L_{AQ} are mutual inductances [pu]; l_{d}, l_{q}, l_{F}, l_{D}, and l_{Q} are leakage inductances [pu]; R_{S}, R_{F}, R_{D}, and R_{Q} are stator, field, d-axis damping, and q-axis damping winding resistances [pu]; H is an inertia constant [s]; and ω_{s} is electric synchronous speed [rad s^{-1}]. All variables are normalized on the base quantities except the electric rotor angle $\delta(t)$ having unit [rad].

The seventh-order model is the superior one; although, on the other hand, it is too complicated to gain insight into the physical characteristics of the controlled plant [5]. It is also not suitable for the design and synthesis of control systems, since many control methods require linear mathematical models for the development of the control system. Many simplified models are derived from this seventh-order nonlinear model [6]. For a synchronous generator analysis and for the design of the PSS control system, a simplified linearized third-order model is still the most popular. It was presented for the first time in 1952 [7] and is, therefore, also called the Heffron-Phillips model.

The Heffron-Phillips model is obtained from the seventh-order nonlinear model by means of linearization for an every steady-state operating point (i.e., an equilibrium point). The Heffron-Phillips model describes the synchronous generator's dynamics in the proximity of the selected equilibrium point. The Heffron-Phillips model has two inputs and three state-space variables. The inputs are mechanical torque $T_{\mathrm{m}\Delta}(t)$ and rotor excitation winding voltage $E_{\mathrm{fd}\Delta}(t)$ deviations; the state-space variables are rotor angle $\delta_{\Delta}(t)$, rotor speed $\omega_{\Delta}(t)$, and voltage behind transient reactance $E'_{\mathrm{q}\Delta}(t)$ deviations. Additional outputs are electric power $P_{\mathrm{e}\Delta}(t)$ and terminal stator voltage $V_{\mathrm{t}\Delta}(t)$ deviations. All the inputs and the state-space variables

denote the deviations (subscript $_\Delta$) from the equilibrium state. The model is written as follows:

$$
\begin{bmatrix} \dot{\delta}_\Delta(t) \\ \dot{\omega}_\Delta(t) \\ \dot{E}'_{q\Delta}(t) \end{bmatrix} = \begin{bmatrix} 0 & \omega_s & 0 \\ -\dfrac{K_1}{2H} & -\dfrac{D}{2H} & -\dfrac{K_2}{2H} \\ -\dfrac{K_4}{T'_{d0}} & 0 & -\dfrac{1}{K_3 T'_{d0}} \end{bmatrix} \begin{bmatrix} \delta_\Delta(t) \\ \omega_\Delta(t) \\ E'_{q\Delta}(t) \end{bmatrix} + \begin{bmatrix} 0 & 0 \\ \dfrac{1}{2H} & 0 \\ 0 & \dfrac{1}{T'_{d0}} \end{bmatrix} \begin{bmatrix} T_{m\Delta}(t) \\ E_{fd\Delta}(t) \end{bmatrix}
$$

(18)

$$
\begin{bmatrix} P_{e\Delta}(t) \\ V_{t\Delta}(t) \end{bmatrix} = \begin{bmatrix} K_1 & 0 & K_2 \\ K_5 & 0 & K_6 \end{bmatrix} \begin{bmatrix} \delta_\Delta(t) \\ \omega_\Delta(t) \\ E'_{q\Delta}(t) \end{bmatrix} + \begin{bmatrix} 0 & 0 \\ 0 & 0 \end{bmatrix} \begin{bmatrix} T_{m\Delta}(t) \\ E_{fd\Delta}(t) \end{bmatrix}
$$

(19)

where $T_{m\Delta}(t)$ represents mechanical torque deviation [pu], $P_{e\Delta}(t)$ is electrical power deviation [pu], $\omega_\Delta(t)$ is rotor speed deviation [pu], $\delta_\Delta(t)$ is rotor angle deviation [rad], $E'_{q\Delta}(t)$ is the voltage behind the transient reactance [pu], $E_{fd\Delta}(t)$ is field excitation voltage deviation [pu], $V_{t\Delta}(t)$ is the terminal voltage [pu], H is an inertia constant [s], D is a damping coefficient representing total lumped damping effects from damper windings [pu/pu], ω_s is rated synchronous speed [rad s^{-1}], T_{do}' is a d-axis transient open circuit time constant [s], and K_1 through K_6 are linearization parameters. All parameters and variables in a Heffron-Phillips model are normalized, except for electric rotor angle $\delta_\Delta(t)$.

3. Analysis of the impact of the oscillations on the power system quality

The oscillations in the power system are due to the physical properties of the synchronous generator that operates parallel to the network. These properties are reflected in the dynamical mathematical model of the synchronous generator and appear as poorly damped dominant eigenvalues. Therefore, any changes in the synchronous generators' inputs (rotor field voltage and mechanical torque), in the network loads (changes in bus voltages) and disturbances, cause oscillations with relatively high amplitude and low damping. Oscillations in the power system are visible in several physical quantities of the system: in the synchronous generators' rotor speed, rotor angle, stator voltage, stator current, and produced power and in the power system's voltages, currents, frequency, and transmitted powers. These oscillations reduce the quality of the electricity and increase the stability risk of the power system.

It is very difficult to estimate the impact of oscillations on actual losses in a power system. In a real power system operation, it is problematic to evaluate how much of the losses is due to the rotor angle oscillations and how much of the losses are due to other factors. Therefore, in the first subsection, the influence of the amplitude and frequency of the oscillations on the amount of the losses in the transmission line and on the constancy of the transmitted power is discussed in more detail. The thoroughly steady-state analysis was made for this purpose. The dynamic analysis is presented in the second subsection. Dynamic analysis shows the vulnerability of the synchronous generator on the different input changes in different operation points.

3.1 Steady-state analysis

An analysis of the impact of the oscillations on losses and on the constancy of the transmitted power is made numerically. In the case of constant rotor speed, the

induced voltage in the stator winding is sinusoidal, with constant amplitude and frequency. The swinging of the rotor speed results in induced voltage with variable frequency and amplitude. From the solution of the swing equation, it is evident that the swinging of the rotor is sinusoidal [8]. Therefore, in a steady-state analysis, we suppose that the rotor's speed oscillates about the constant synchronous speed with sinusoidal oscillations. This results in the stator's induced voltage, which varies sinusoidally in amplitude and frequency. The amplitude increases when the frequency increases, and vice versa. For such input signal, there is no transparent analytical solution for the evaluation of the losses and constancy of the transmitted power. Therefore, the numerical solution that is based on an equivalent circuit of the synchronous generator connected by transmission line to the infinite bus is used for the analysis. The equivalent circuit is shown in **Figure 1**.

where V_{1e} denotes the effective value of the generator's internal voltage [pu], V_{2e} is the effective value of the infinite bus voltage [pu], φ_1 is the generator's internal voltage angle [rad], φ_2 is the infinite bus voltage angle [rad], R_s is stator (armature) resistance [pu], X_s is synchronous reactance [pu], R_e is transmission line resistance [pu], and X_e is transmission line reactance [pu]. The equivalent circuit presented in **Figure 1** is a balanced symmetrical three-phase system. The impedance in any one phase is equal to that in either of the other two phases. Three voltages on the generator side are displaced 120° electrical degrees in time as a result of the phases being displaced 120° in space. Also, the three voltages on the infinite bus side are displaced 120° electrical degrees in time, so that the resulting phase currents are equal in amplitude and displaced in phase from each other by 120°. $v_{1a}(t)$, $v_{1b}(t)$, and $v_{1c}(t)$ denote instantaneous values of the synchronous generator's internal phase voltages; $v_{IBa}(t)$, $v_{IBb}(t)$, and $v_{IBc}(t)$ denote instantaneous values of the infinite bus phase voltages; and $i_a(t)$, $i_b(t)$, and $i_c(t)$ denote instantaneous values of the transmission line phase currents. Unless otherwise specified, $P_{IB}(t)$ represents the instantaneous three-phase power flow to the infinite bus [pu]; $P_{IBa}(t)$, $P_{IBb}(t)$, and $P_{IBc}(t)$ represent instantaneous power flow to the infinite bus for different phases [pu]; and P_{IB} represents the mean value of the instantaneous three-phase power flow to the infinite bus [pu]. $P_L(t)$ denotes instantaneous three-phase power losses
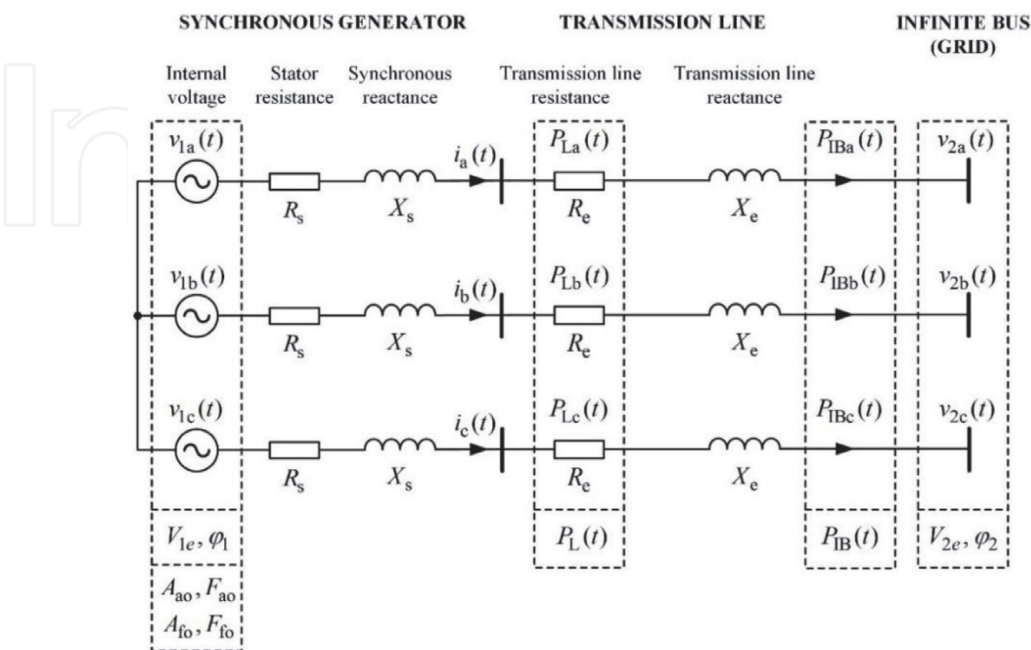

Figure 1.
Equivalent circuit of the synchronous generator connected by transmission line to the infinite bus used for the steady-state analysis.

in the transmission line [pu]; $P_{La}(t)$, $P_{Lb}(t)$, and $P_{Lc}(t)$ represent instantaneous power losses for different phases [pu]; and P_L represents the mean value of the instantaneous three-phase power losses in the transmission line [pu]. p_L indicates the relative value of the mean value of the three-phase power losses (P_L) compared to the mean value of the three-phase power flow to the infinite bus (P_{IB}) in [%]. Stator voltage amplitude and frequency oscillations resulting from rotor speed swing are described with the amplitude and frequency of both oscillations. A_{ao} and F_{ao} denote amplitude and frequency of amplitude oscillations. A_{fo} and F_{fo} denote the amplitude and frequency of frequency oscillations.

For the presented results, the impedances of the synchronous generator and transmission line are shown in **Table 1**.

Figures 2–5 show the time responses of the electrical quantities if there are no oscillations in rotor speed. The parameters of the generator's internal voltage and infinite bus voltage are shown in **Table 2**.

Figure 2 shows the instantaneous values of the synchronous generator's internal voltages for all three phases. Currents in the transmission lines are shown in **Figure 3**. Power flow to the infinite bus for all three phases separately and the sum of the phases' power flow are shown in **Figure 4**. As expected, the total three-phase power flow is constant. **Figure 5** shows power losses in the transmission line for all three phases separately and the three-phase power losses. Again, the total three-phase power losses are constant.

Figures 6–10 show the time responses of the electrical quantities if oscillations occur in the rotor speed. The parameters of the generator's internal voltage and infinite bus voltage are shown in **Table 3**.

R_a = 0.0011 [pu]	X_s = 0.9 [pu]
R_e = 0.02 [pu]	X_e = 0.4 [pu]

Table 1.
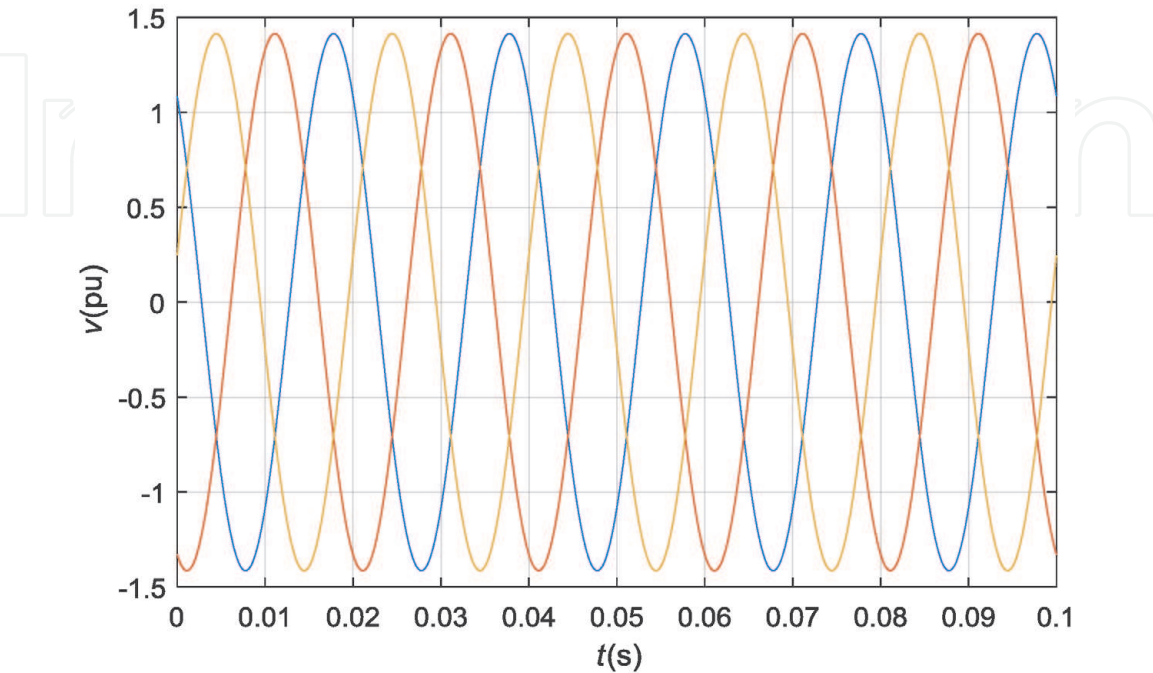*The synchronous generator's and transmission line's impedances.*

Figure 2.
Synchronous generator's internal voltages for all three phases: $v_{1a}(t)$, $v_{1b}(t)$, and $v_{1c}(t)$.
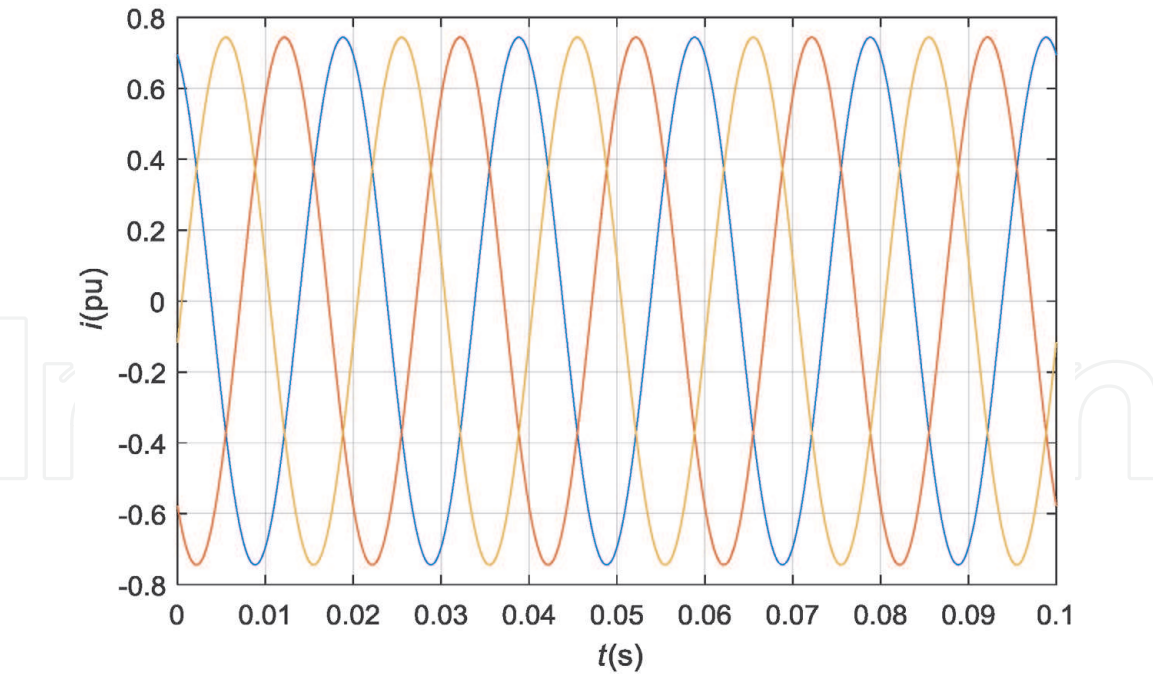
Figure 3.
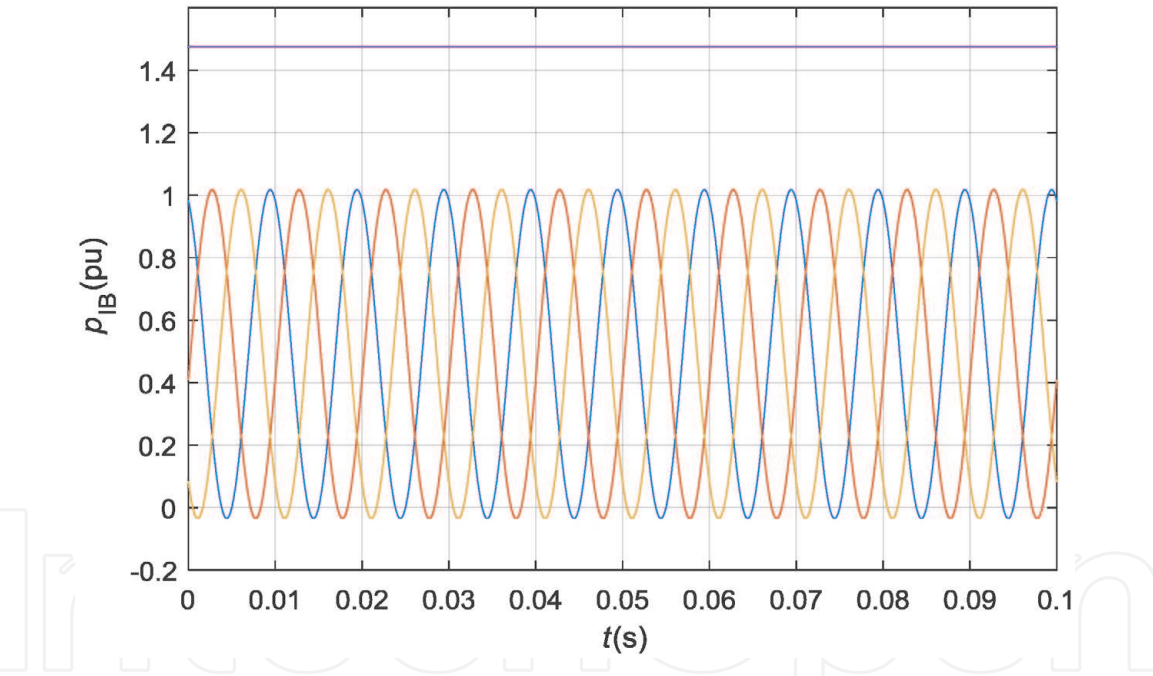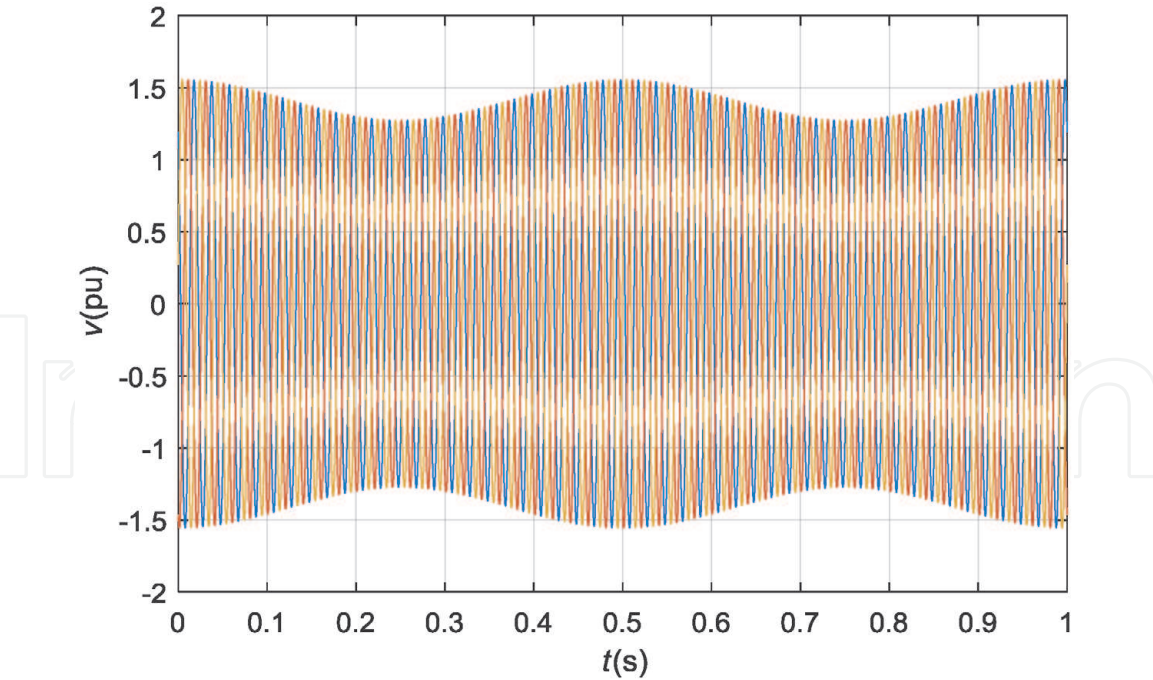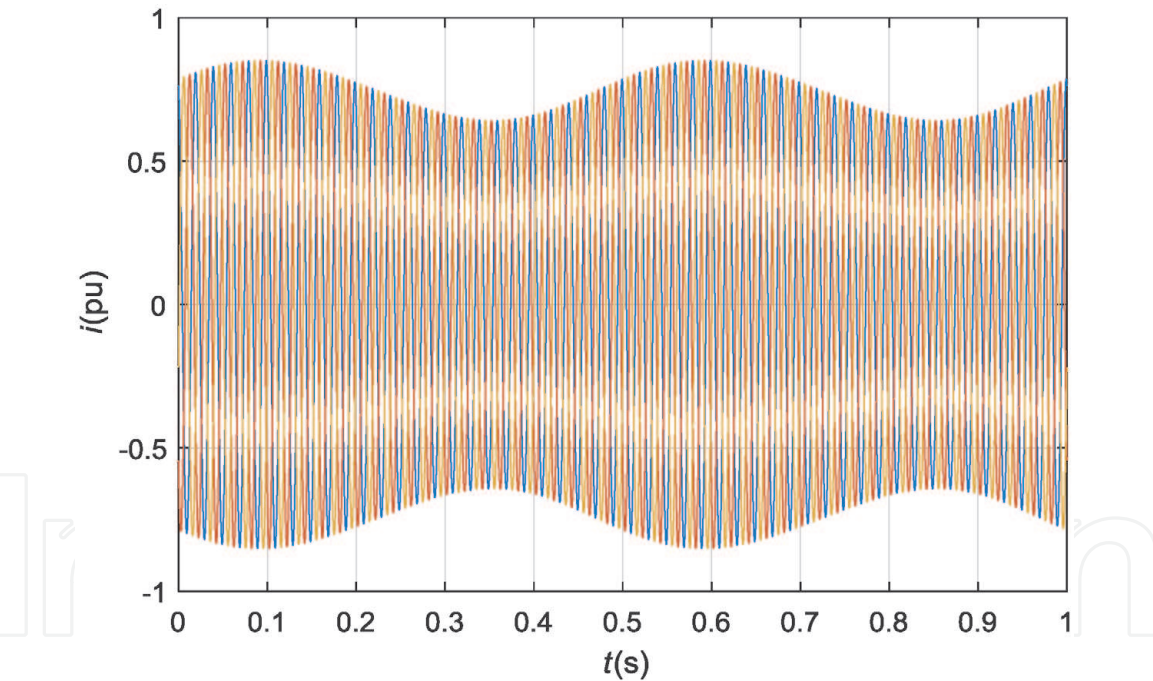*Transmission line currents for all three phases: $i_a(t)$, $i_b(t)$, and $i_c(t)$.*

Figure 4.
Instantaneous three-phase power flow to the infinite bus $P_{IB}(t)$ (constant), and instantaneous power flow to the infinite bus for different phases $P_{IBa}(t)$, $P_{IBb}(t)$, and $P_{IBc}(t)$.

For better insight, **Figure 6** shows the instantaneous values of the synchronous generator's internal voltage for phase a. The oscillations are visible in amplitude and in frequency.

Figure 7 shows the instantaneous values of the synchronous generator's internal voltages for all three phases. Currents in the transmission lines are shown in **Figure 8**. Power flow to the infinite bus for all three phases separately and the instantaneous value of the three-phase power flow are shown in **Figure 9**. In this case, due to oscillations in rotor speed, and, consequently, oscillations in the internal voltages, the total three-phase power flow is not constant. **Figure 10** shows power losses in the transmission line for all three phases separately and the three-phase power losses. Again, total three-phase power losses are not constant.
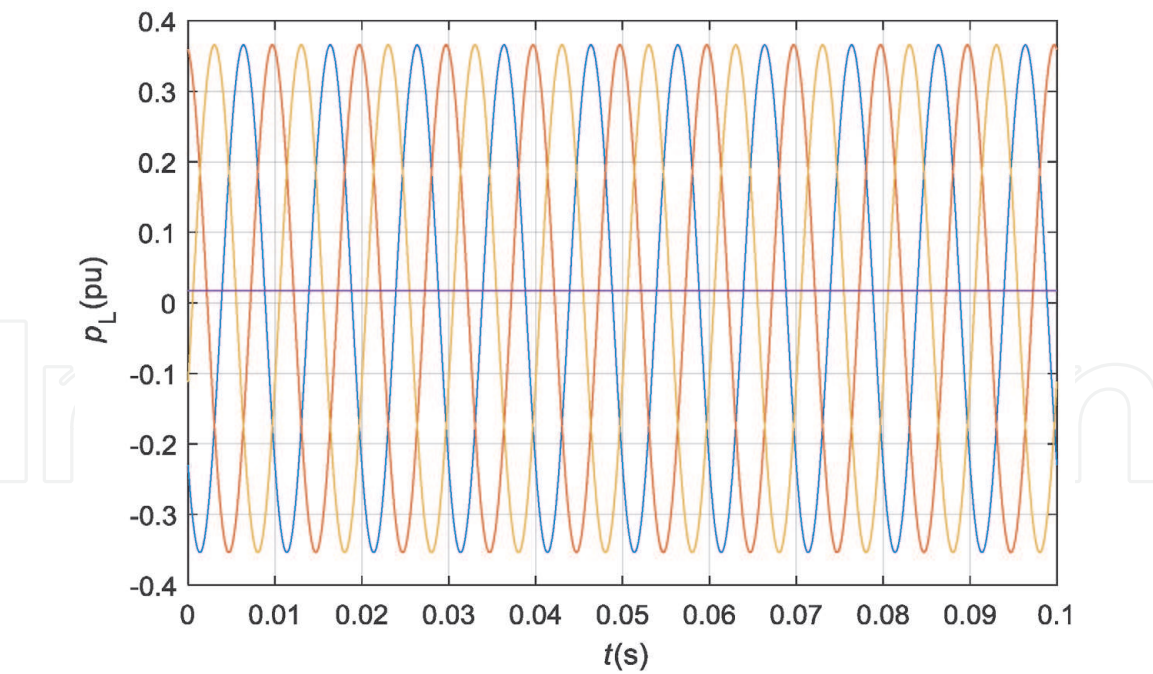
Figure 5.
Instantaneous three-phase power losses in the transmission line $P_L(t)$ *(constant) and instantaneous power losses in the transmission line for different phases* $P_{IBa}(t)$, $P_{IBb}(t)$, *and* $P_{IBc}(t)$.

V_{1e} = 1.0 [pu]		φ_1 = 40 [°]
V_{2e} = 1.0 [pu]		φ_1 = 0 [°]
A_{ao} = 0.0 [pu]		F_{ao} = 0 [Hz]
A_{fo} = 0.0 [pu]		F_{fo} = 0 [Hz]

Table 2.
The parameters of the internal voltage and infinite bus voltage, without oscillations.
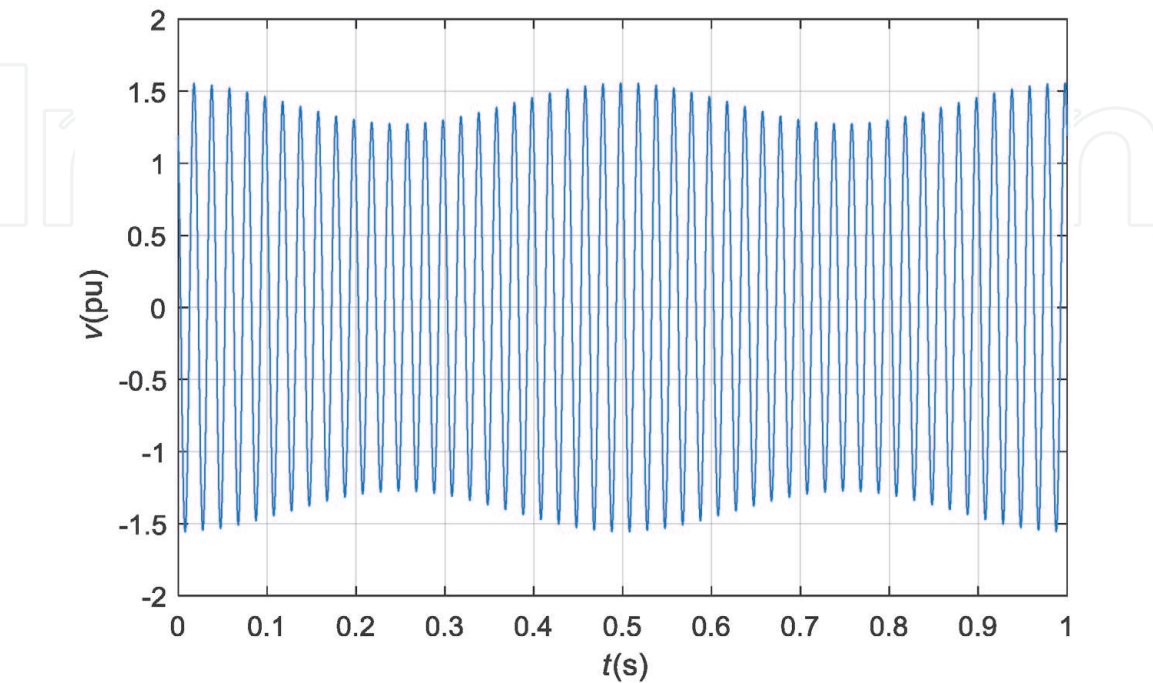
Figure 6.
Synchronous generator's internal voltages for phase a: $v_{1a}(t)$.

9

Figure 7.
Synchronous generator's internal voltages for all three phases: $v_{1a}(t)$, $v_{1b}(t)$, and $v_{1c}(t)$.

Figure 8.
Transmission line currents for all three phases: $i_a(t)$, $i_b(t)$, and $i_c(t)$.

From **Figures 2–10**, it is seen clearly that the rotor speed oscillations cause the oscillation in the transmitted power. The sum of the transmitted powers of the individual phases is no longer constant (**Figure 9**), as is the case for the balanced three-phase symmetric systems without oscillations (**Figure 4**). These oscillations reduce the transmission capability and quality. To ensure the power transmission with minimal power oscillations, it is necessary to reduce the rotor speed oscillations.

A thorough numerical analysis was performed to estimate the influence of the rotor speed oscillations on the power system losses. Some results are presented in **Tables 4** and **5**. **Table 4** shows the impact of the rotor speed oscillations on the
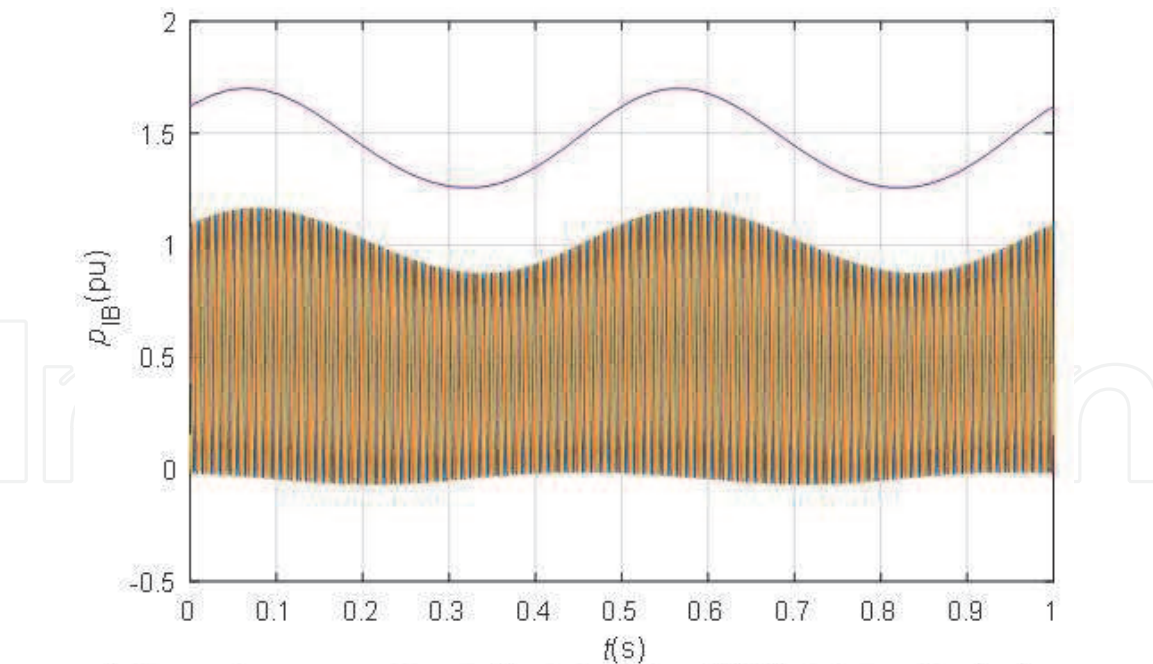
Figure 9.
Three-phase power flow to the infinite bus $P_{IB}(t)$ (violet) and instantaneous power flow to the infinite bus for different phases $P_{IBa}(t)$, $P_{IBb}(t)$, and $P_{IBc}(t)$.
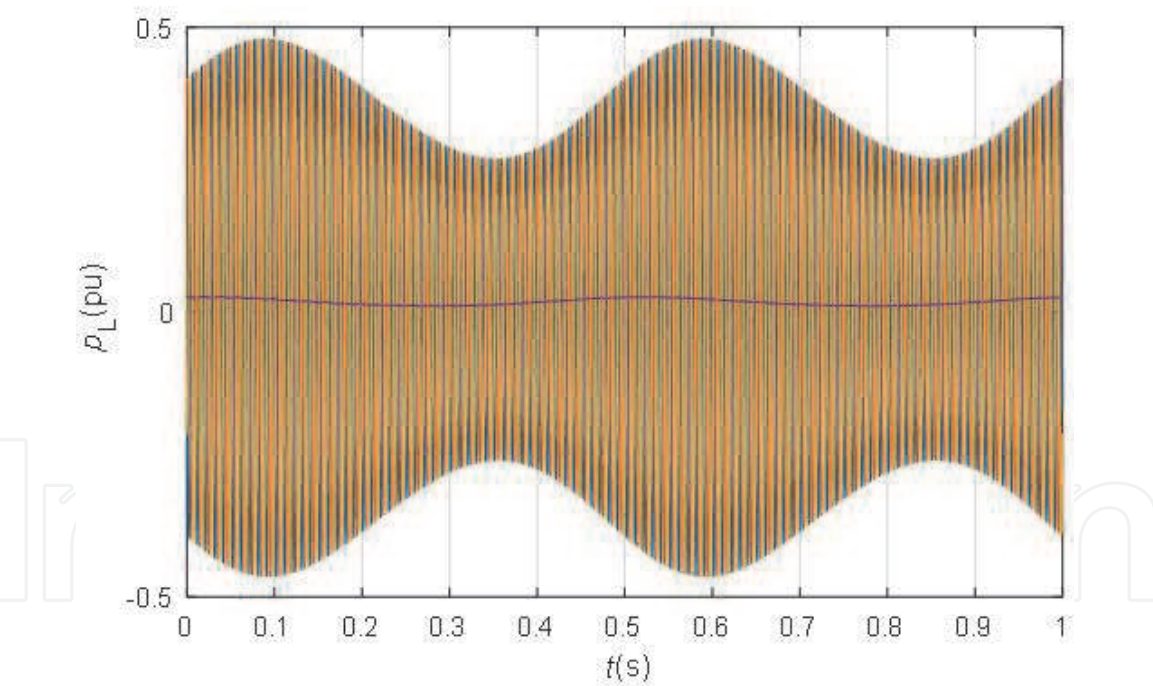

Figure 10.
Three-phase power losses in the transmission line $P_L(t)$ (violet) and instantaneous power losses in the transmission line for different phases $P_{IBa}(t)$, $P_{IBb}(t)$, and $P_{IBc}(t)$.

$V_{1e} = 1.0$ [pu]	$\varphi_1 = 40$ [°]
$V_{2e} = 1.0$ [pu]	$\varphi_1 = 0$ [°]
$A_{ao} = 0.1$ [pu]	$F_{ao} = 2$ [Hz]
$A_{fo} = 0.1$ [pu]	$F_{fo} = 2$ [Hz]

Table 3.
The parameters of the internal voltage and infinite bus voltage, with oscillations in internal voltage.

losses by active power generation. The results are presented in two different operating points. In the first one, the electric angle between generator internal voltage and infinite bus voltage was 10°, and, in the second one, the angle amounts to 40°. The results of the rotor speed oscillations' variations are presented in the amplitude range from 0 to 20% of the synchronous speed by frequencies 1 and 2 [Hz]. From the obtained results, it is evident that there is no influence of the oscillations on power losses in the transmission line.

Table 5 shows the impact of the rotor speed oscillations on the losses by reactive power generation. The results are presented at two different operating points. In the first one, the generator's internal voltage was 10% bigger than the infinite bus voltage, and, in the second one, the difference amounts to 50%. The results of rotor speed oscillations' variations are presented in the amplitude range from 0 to 20% of the synchronous speed by frequencies 1 and 2 [Hz]. From the results, it is obvious

V_{1e}	V_{2e}	φ_1	φ_2	A_{ao}	A_{fo}	F_{ao}	F_{fo}	P_{IB}	P_L	p_L
1.0	1.0	10	0	0.0	0.0	0	0	0.40	$1.1 \cdot 10^{-3}$	0.3
1.0	1.0	10	0	0.1	0.1	1	1	0.40	$1.5 \cdot 10^{-3}$	0.4
1.0	1.0	10	0	0.1	0.1	2	2	0.40	$1.5 \cdot 10^{-3}$	0.4
1.0	1.0	10	0	0.2	0.2	1	1	0.40	$2.6 \cdot 10^{-3}$	0.6
1.0	1.0	10	0	0.2	0.2	2	2	0.40	$2.5 \cdot 10^{-3}$	0.6
1.0	1.0	40	0	0.0	0.0	1	1	1.47	$1.8 \cdot 10^{-2}$	1.2
1.0	1.0	40	0	0.1	0.1	1	1	1.47	$1.8 \cdot 10^{-2}$	1.2
1.0	1.0	40	0	0.1	0.1	2	2	1.46	$1.9 \cdot 10^{-2}$	1.3
1.0	1.0	40	0	0.2	0.2	1	1	1.46	$1.9 \cdot 10^{-2}$	1.3
1.0	1.0	40	0	0.2	0.2	2	2	1.46	$1.9 \cdot 10^{-2}$	1.3

Table 4.
Mean values of three-phase transmitted power to the infinite bus (P_{IB}) and three-phase power losses in the transmission line P_L as a function of the angle between the generator's internal voltage and infinite bus voltage (φ_1-φ_2) by different amplitudes (A_{ao}, A_{fo}) and frequencies (F_{ao}, F_{fo}) of amplitude and frequency oscillations in the generator's internal voltage by active power transmission.

V_{1e}	V_{2e}	φ_1	φ_2	A_{ao}	A_{fo}	F_{ao}	F_{fo}	P_{IB}	P_L	p_L
1.1	1.0	0	0	0.0	0.0	0	0	$3.7 \cdot 10^{-3}$	$3.7 \cdot 10^{-4}$	10
1.1	1.0	0	0	0.1	0.1	1	1	$3.6 \cdot 10^{-3}$	$7.9 \cdot 10^{-4}$	22
1.1	1.0	0	0	0.1	0.1	2	2	$3.6 \cdot 10^{-3}$	$7.7 \cdot 10^{-4}$	21
1.1	1.0	0	0	0.2	0.2	1	1	$3.3 \cdot 10^{-3}$	$2.0 \cdot 10^{-3}$	61
1.1	1.0	0	0	0.2	0.2	2	2	$3.3 \cdot 10^{-3}$	$2.0 \cdot 10^{-3}$	61
1.5	1.0	0	0	0.0	0.0	0	0	$1.9 \cdot 10^{-2}$	$9.4 \cdot 10^{-3}$	50
1.5	1.0	0	0	0.1	0.1	1	1	$1.9 \cdot 10^{-2}$	$1.0 \cdot 10^{-2}$	54
1.5	1.0	0	0	0.1	0.1	2	2	$1.9 \cdot 10^{-2}$	$1.0 \cdot 10^{-2}$	54
1.5	1.0	0	0	0.2	0.2	1	1	$1.8 \cdot 10^{-2}$	$1.2 \cdot 10^{-2}$	66
1.5	1.0	0	0	0.2	0.2	2	2	$1.8 \cdot 10^{-2}$	$1.2 \cdot 10^{-2}$	66

Table 5.
Mean values of three-phase transmitted power to the infinite bus (P_{IB}) and three-phase power losses in the transmission line P_L as a function of the generator's internal voltage (V_{1e}) by different amplitudes (A_{ao}, A_{fo}) and frequencies (F_{ao}, F_{fo}) of amplitude and frequency oscillations in the generator's internal voltage by reactive power transmission.

that the influence of the oscillations on power losses in the transmission line is negligible.

3.2 Dynamic analysis

The Heffron-Phillips model described in Section 2 is used for the analysis of the dynamic characteristics of the synchronous generator. The impact of the inputs' variations on the oscillations is studied on the synchronous generator with the following data [4]:

New parameters in **Table 6** are as follows: S_N is nominal power [MVA], V_N is nominal voltage [kV], $\cos \varphi_N$ is a nominal power factor, and x'_d is unsaturated d-axis transient reactance [pu].

From the data in **Table 6**, the equilibrium state for the Heffron-Phillips model is calculated by means of a phasor diagram. Phasor equations permit the solution of the initial conditions that exist prior to the application of the inputs' variations. The linearization coefficients of the Heffron-Phillips model are calculated for the synchronous generator with data in **Table 6** and for the calculated equilibrium state's data. The linearization coefficients for nominal operating point (P_N = 1 [pu], $\cos \varphi_N$ = 0.85), and eigenvalues of the Heffron-Phillips model (λ_1, λ_2, and λ_3) are presented in **Table 7**.

The linearized Heffron-Phillips model of a synchronous generator has three eigenvalues. The damping ratio and frequency of rotor angle oscillation are seen directly from the dominant conjugate complex eigenvalues. Therefore, it is very transparent to investigate the dependence of the synchronous generator's oscillation dynamics from the operating point by means of eigenvalue analysis. By changing the operating point, the Heffron-Phillips model's eigenvalues also change.

Transient response of the synchronous generator with data in **Table 6** and nominal operating point with data in **Table 7** are shown in **Figures 11–13**. Step changes are simulated in both generator's inputs. **Figure 11** shows the simulated

S_N = 160 [MVA]	V_N = 15 [kV]	$\cos \varphi_N$ = 0.85
ω_s = 377 [rad s^{-1}]		
T'_{d0} = 5.9 [pu]	H = 2.37 [s]	D = 2.0 [pu]
R_e = 0.02 [pu]	L_e = 0.4 [pu]	V_{IB} = 1.0 [pu]
R_s = 0.0011 [pu]	R_F = 0.0007 [pu]	x'_d = 0.245 [pu]
L_d = 1.700 [pu]	L_q = 1.640 [pu]	L_F = 0.101 [pu]
L_D = 0.055 [pu]	L_Q = 0.036 [pu]	L_{AD} = 1.550 [pu]
l_d = 0.150 [pu]	l_q = 0.150 [pu]	L_{AQ} = 1.490 [pu]

Table 6.
Data of the synchronous generator used for dynamic analysis [4].

P_N = 1.0 [pu]	Q_N = 0.62 [pu]	$\cos \varphi_N$ = 0.85
K_1 = 1.4478	K_2 = 1.3174	K_3 = 0.3072
K_4 = 1.8052	K_5 = 0.0294	K_6 = 0.5257
λ_1 = −0.3502 + 10.7270i	λ_2 = −0.3502 − 10.7270i	λ_3 = −0.2732

Table 7.
Linearization parameters and eigenvalues of the Heffron-Phillips model in the nominal operating point.

trajectory of the turbine mechanical torque and rotor excitation voltage. Step changes are selected in order to maximize the excitation of oscillations.

The responses of the generated electrical power and the stator voltage are shown in **Figure 12**. The oscillations are seen clearly from the response of the generated electrical power.

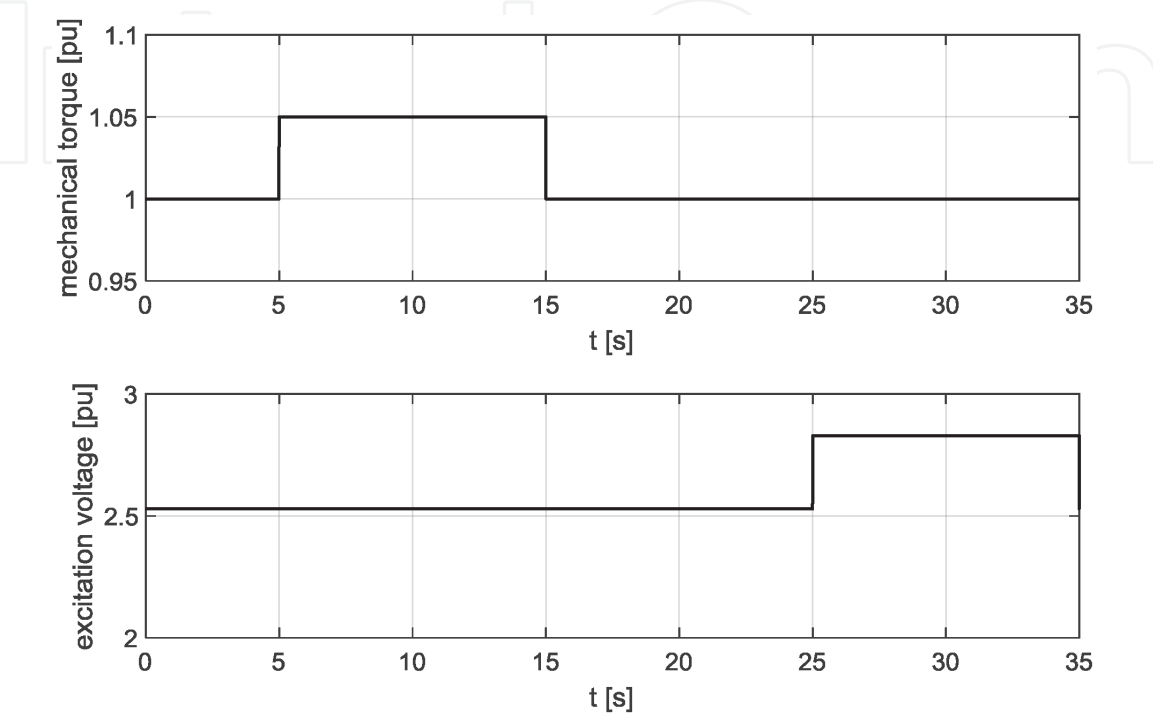**Figure 13** shows the response of the rotor speed and rotor angle on the inputs' trajectories shown in **Figure 11**.

Figure 11.
Synchronous generator inputs' trajectories: Mechanical torque T_m(t) [pu] and rotor excitation voltage E_{fd}(t) [pu], nominal operating point P = 1.0 [pu] and Q = 0.62 [pu].
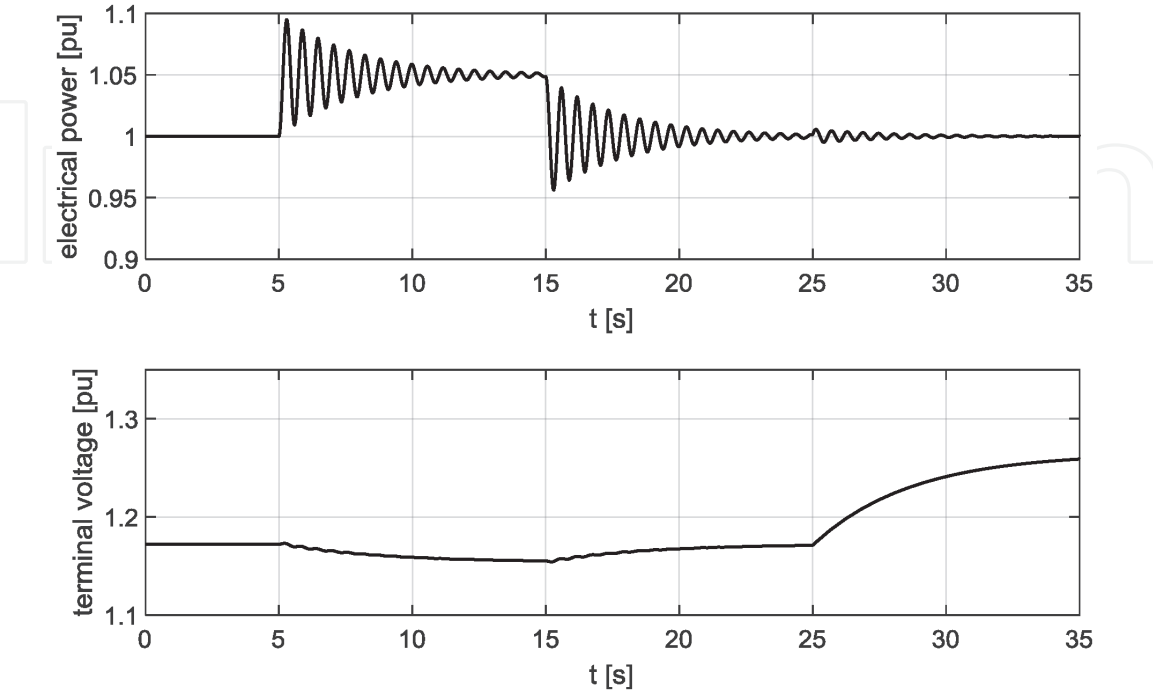
Figure 12.
Synchronous generator outputs' trajectories: Generated electrical power P_e(t) [pu] and stator terminal voltage V_t(t) [pu], nominal operating point P = 1.0 [pu] and Q = 0.62 [pu].
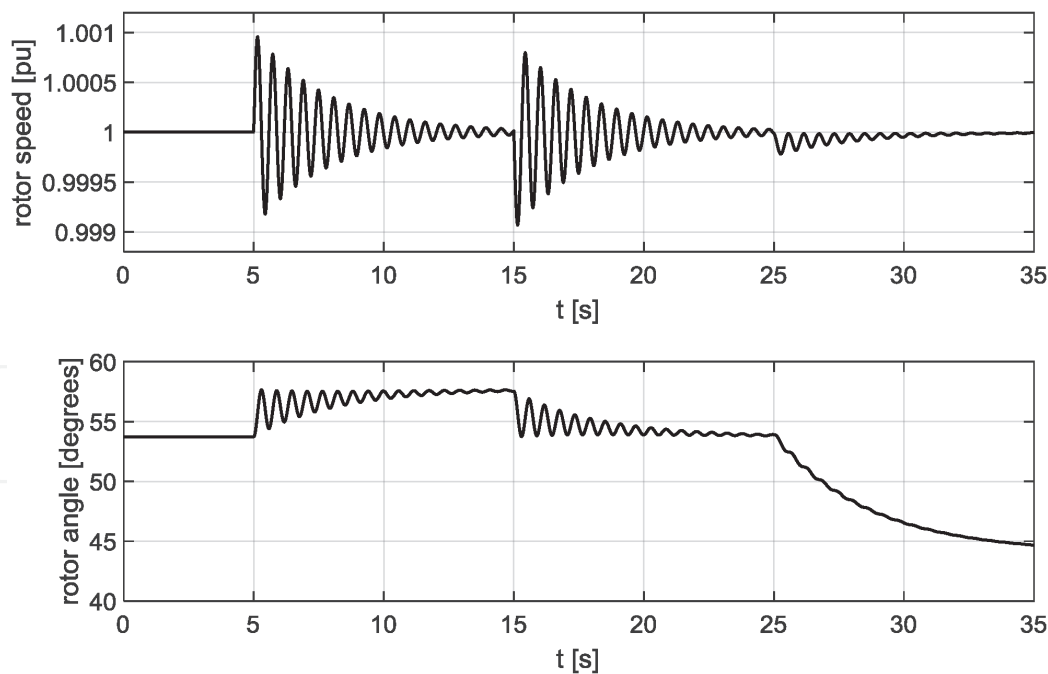
Figure 13.
Synchronous generator outputs' trajectories: Rotor speed ω(t) [pu] and rotor angle δ(t) [degrees], nominal operating point P = 1.0 [pu] and Q = 0.62 [pu].

P = 1.0 [pu]	Q = 0.1 [pu]	cos φ = 0.995
K_1 = 1.2506	K_2 = 1.5867	K_3 = 0.3072
K_4 = 2.2164	K_5 = −0.0730	K_6 = 0.3693
$λ_1$ = −0.4493 + 9.9715i	$λ_2$ = −0.4493 − 9.9715i	$λ_3$ = −0.0750

Table 8.
Linearization parameters and eigenvalues of the Heffron-Phillips model at operating point P = 1.0 [pu] and Q = 0.1 [pu].

To evaluate the influence of the operating point on the synchronous generator's dynamics, the Heffron-Phillips model was calculated, and simulations were performed at different operating points for different types of generators with different nominal values. From the obtained results, it was obvious that the dynamics of the synchronous generator vary significantly.

In this text, results for the synchronous generator with data in **Table 6** are presented for the two most distinctive operating points:

- The operating point with high active power and low reactive power: *P* = 1.0 [pu] and *Q* = 0.1 [pu]. This point represents the strongly damped operating point and, therefore, the less problematic case for testing of the PSS.

- The operating point with low active power and high reactive power *P* = 0.1 [pu] and *Q* = 1.0 [pu]. This point represents the weakly damped real operating point and, therefore, the worst case for testing of the PSS.

Table 8 shows the linearization data and Heffron-Phillips model eigenvalues for the operating point where active power is generated with very high power factor cos *φ*.

The results of the simulation of the synchronous generator at operating point *P* = 1 [pu] and *Q* = 0.1 [pu] are shown in **Figures 14–16**.

Table 9 shows the linearization data and Heffron-Phillips model eigenvalues for other interesting operating points. In this case, almost only reactive power is generated—Power factor cos φ is very small.

The results of the simulation of the synchronous generator in operating point $P = 0.1$ [pu] and $Q = 1.0$ [pu] are shown in **Figures 17–19**.
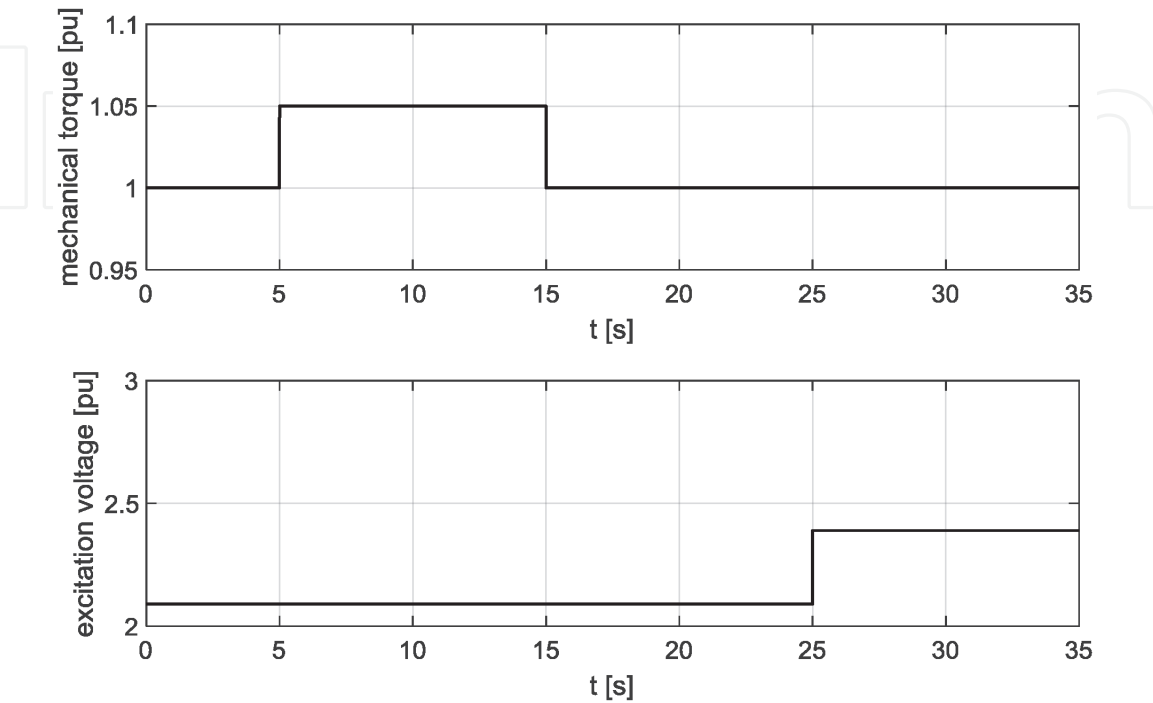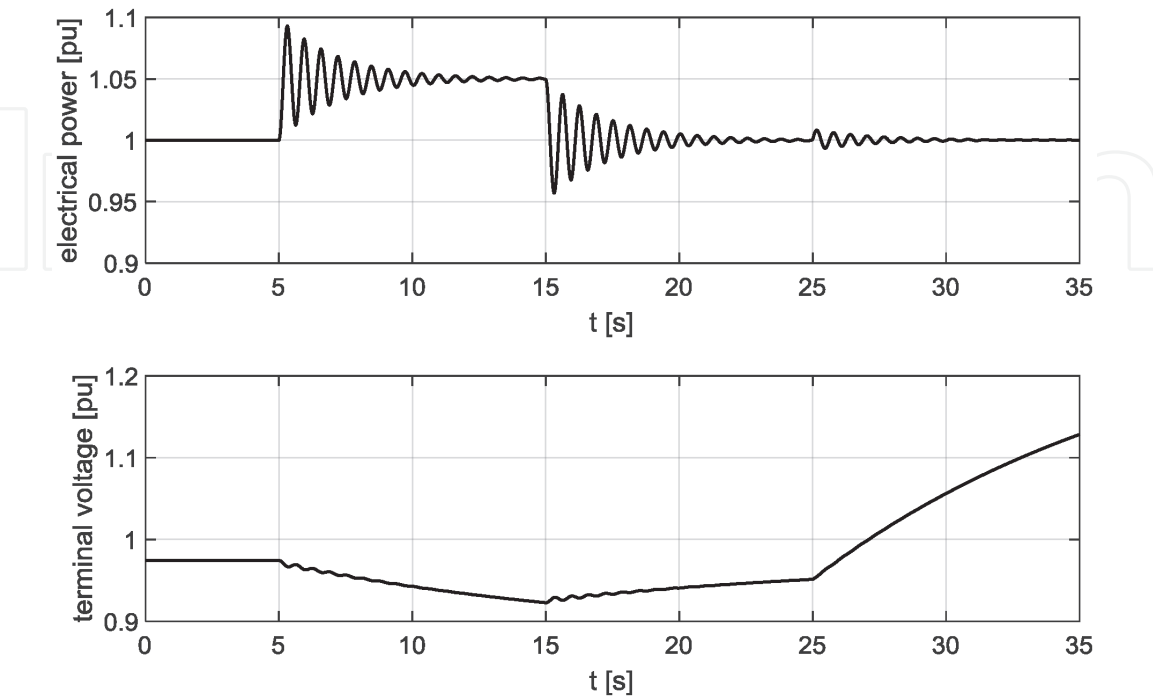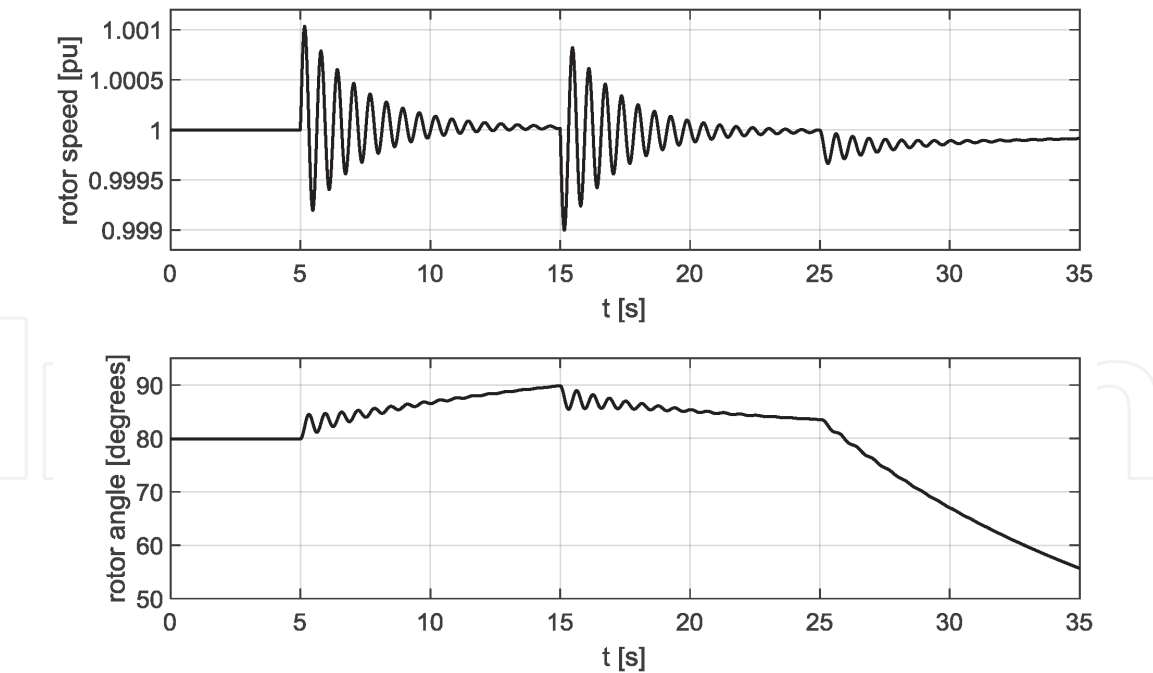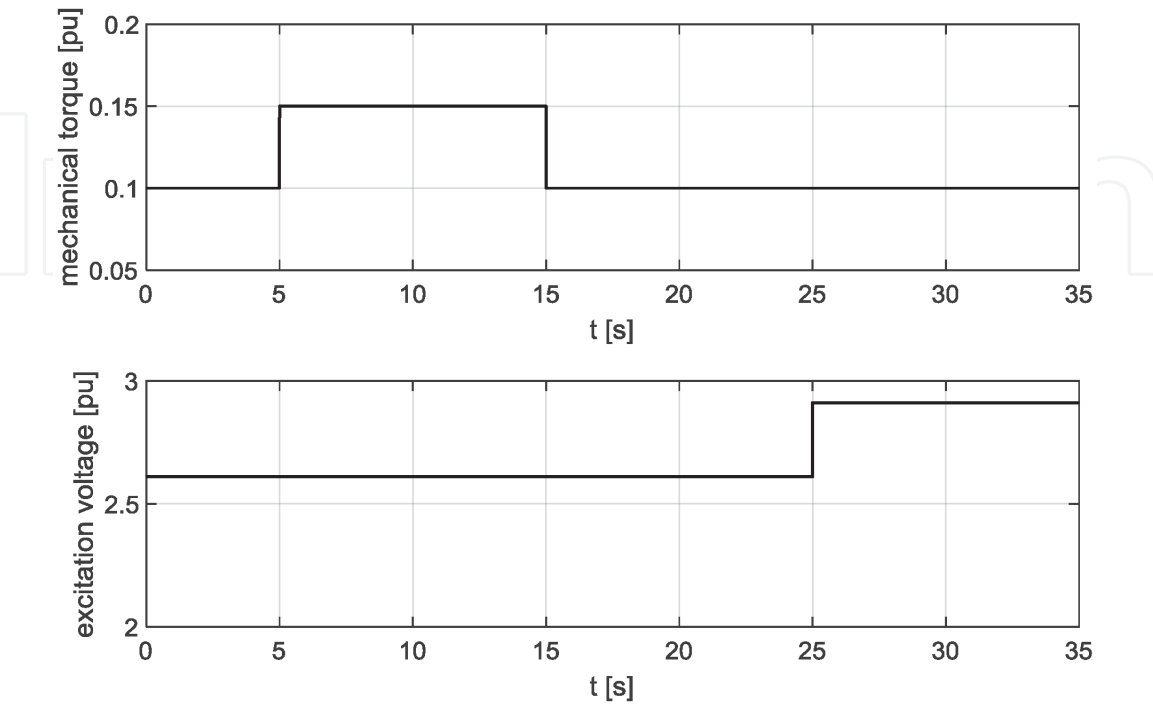

Figure 14.
Synchronous generator inputs' trajectories: Mechanical torque $T_m(t)$ *[pu] and rotor excitation voltage* $E_{fd}(t)$ *[pu], operating point P = 1.0 [pu] and Q = 0.1 [pu].*
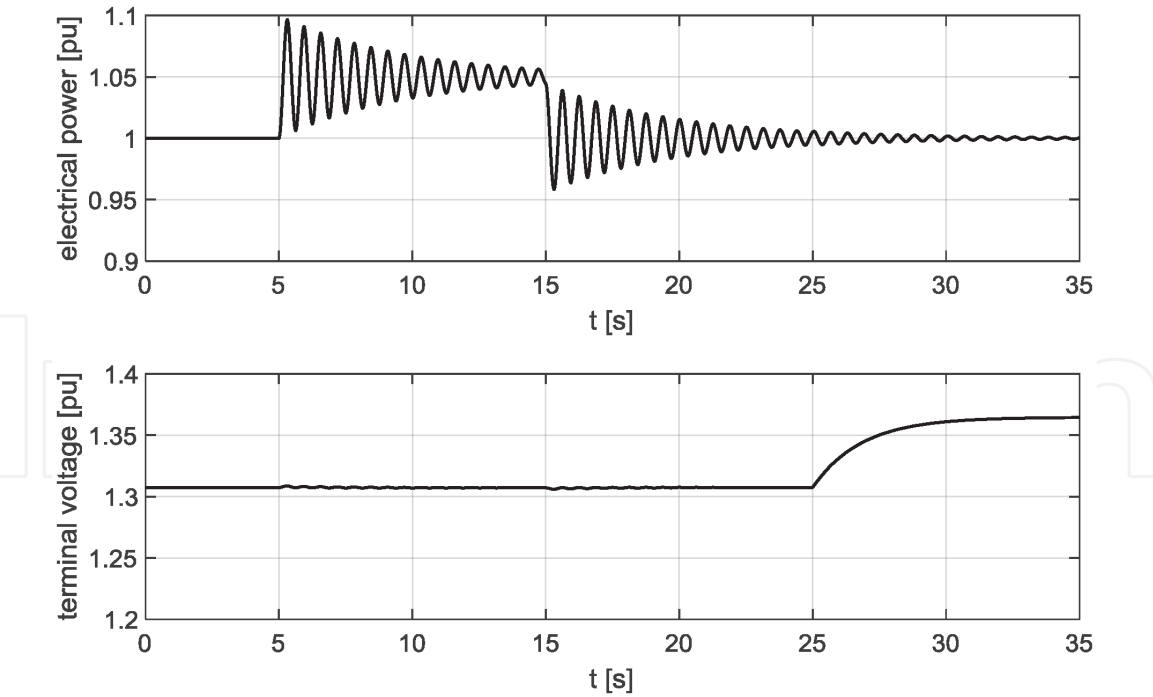

Figure 15.
Synchronous generator outputs' trajectories: Generated electrical power $P_e(t)$ *[pu] and stator terminal voltage* $V_t(t)$ *[pu], operating point P = 1.0 [pu] and Q = 0.1 [pu].*

Figure 16.
Synchronous generator outputs' trajectories: Rotor speed ω(t) [pu] and rotor angle δ(t) [degrees], operating point P = 1.0 [pu] and Q = 0.1 [pu].

P = 0.1 [pu]	Q = 1.0 [pu]	cos φ = 0.099
K_1 = 1.2614	K_2 = 0.1631	K_3 = 0.3072
K_4 = 0.1219	K_5 = 0.0185	K_6 = 0.6207
λ_1 = −0.2123 + 10.0141i	λ_2 = −0.2123 − 10.0141i	λ_3 = −0.5490

Table 9.
Linearization parameters and eigenvalues of the Heffron-Phillips model at operating point P = 0.1 [pu] and Q = 1.0 [pu].

Figure 17.
Synchronous generator inputs' trajectories: Mechanical torque T_m(t) [pu] and rotor excitation voltage E_{fd}(t) [pu], operating point P = 0.1 [pu] and Q = 1.0 [pu].

Figure 18.
Synchronous generator outputs' trajectories: Generated electrical power $P_e(t)$ [pu] and stator terminal voltage $V_t(t)$ [pu], operating point P = 0.1 [pu] and Q = 1.0 [pu].
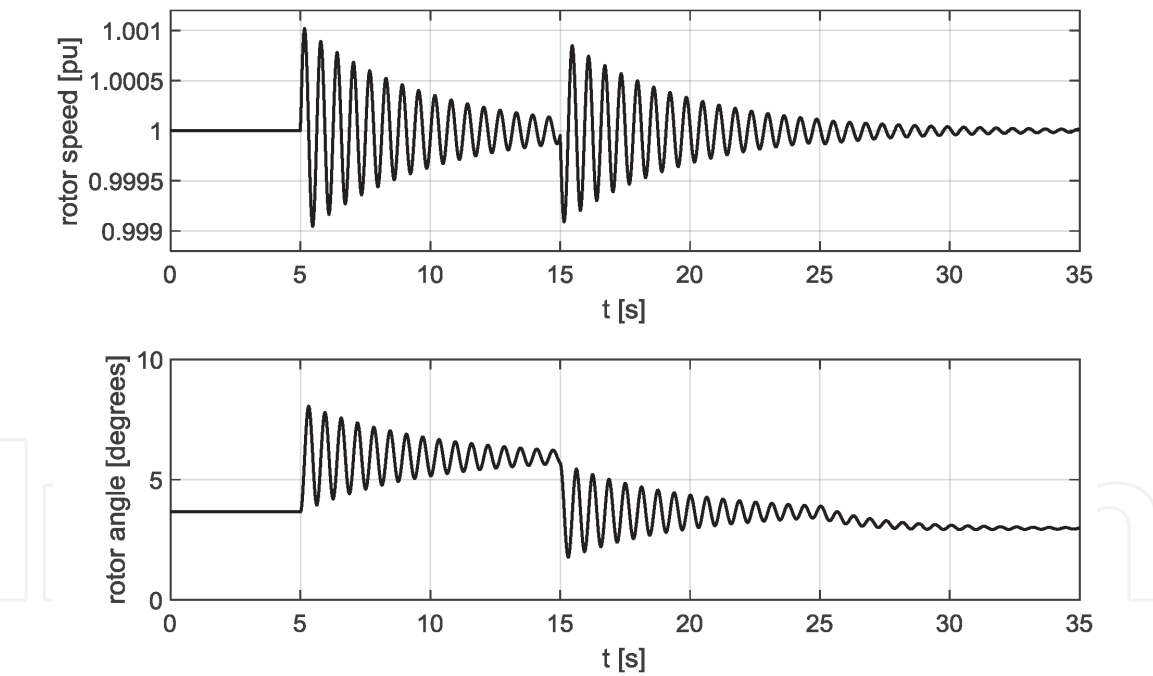

Figure 19.
Synchronous generator outputs' trajectories: Rotor speed $\omega(t)$ [pu] and rotor angle $\delta(t)$ [degrees], operating point P = 0.1 [pu] and Q = 1.0 [pu].

From the analysis of the effect of different loadings on the synchronous generator dynamic characteristics, it can be concluded that the variations in the machine dynamics are considerable in the entire operating range, and, therefore, a control system is necessary for damping of the oscillations. From the comparison of the responses across different operating points, it is obvious that the present system is nonlinear and that the conventional linear control theory does not provide adequate damping throughout the entire operating area. Therefore, the implementation of a robust or adaptive control theory is meaningful.

4. Conventional control system for synchronous generator's rotor excitation equipment

Two principal control systems affect a synchronous generator directly: a governor control system and an excitation control system. The governor control system controls the mechanical power from a steam or water turbine by opening or closing valves regulating the steam or water flow. The response of the governor control system is too slow to damp the synchronous generator's oscillations, which are mainly in the frequency range 0.5–2.5 Hz. Damping the oscillations is possible only with the excitation control system. The excitation control system (also called an automatic voltage regulator) changes the rotor field voltage (and current) in such a way that the generator's output voltage is the same (or close enough) to the reference voltage. In modern power plants, the thyristor or transistor rectifiers are used mainly to generate the required voltage for rotor winding. The electrical power flow from the excitation system is much smaller than the mechanical power flow. This, and the fact that semiconductor components are used in the excitation system instead of mechanical ones, is the reason that the excitation system is significantly faster than the governor system. Therefore, an exciter is used for the damping of the oscillations.

A conventional linear PSS approach is based on utilization of the static excitation system. Through this system, the PSS changes the field excitation voltage of a synchronous generator. An additional component of an electrical torque is generated as a consequence. This torque must be in phase with the rotor speed and thus increases damping of the synchronous generator [9]. **Figure 20** presents a block diagram of the Heffron-Phillips model of synchronous generator equipped with an excitation system, voltage controller, and power system stabilizer [10]. The generator's output voltage is compared with a reference voltage, and the calculated error is driven to the rectifier with an integrated voltage controller. The rectifier with the voltage controller is presented with the first-order model. The PSS input represents one or more signals in which oscillations are visible. The PSS generates an additional signal, which is added to the voltage error.
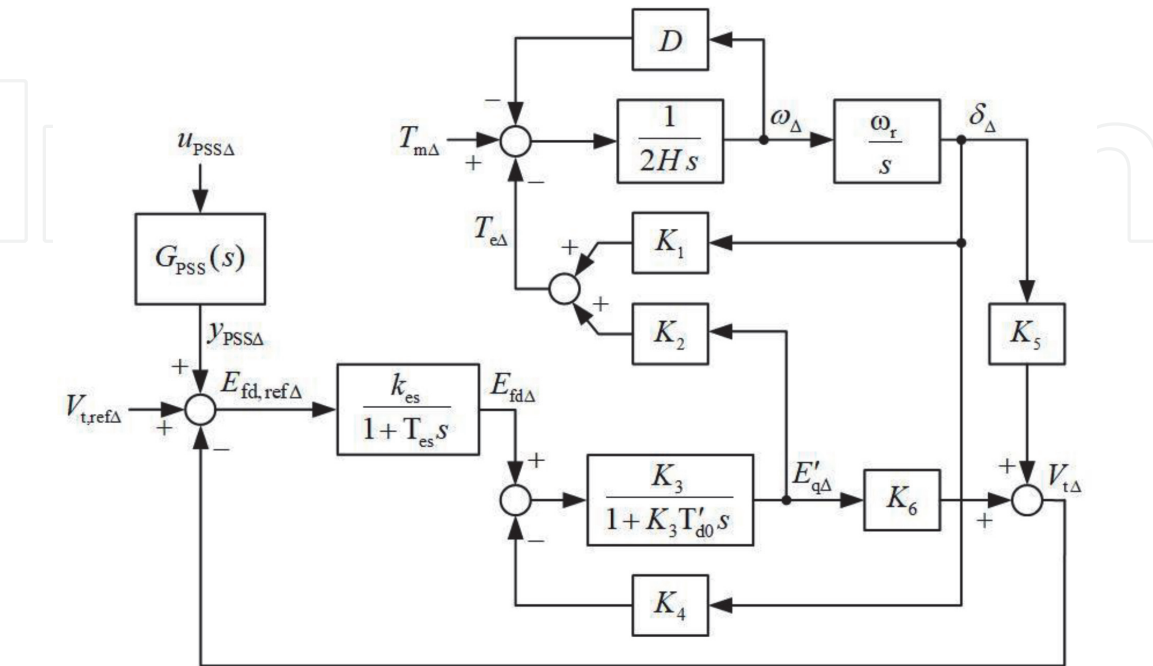

Figure 20.
Block diagram of the Heffron-Phillips model of synchronous generator equipped with excitation system, voltage controller, and power system stabilizer.

The symbols in **Figure 20** represent the following: k_{es} and T_{es} are the excitation system gain [pu.] and the time constant [s], respectively, $E_{fd,ref}$ is the reference for field excitation voltage E_{fd} (both in [pu]), while u_{PSS}, y_{PSS}, and $G_{PSS}(s)$ are the PSS input, the output (both in [pu]), and the transfer function, respectively. As for the variables of the Heffron-Phillips model, subscript $_\Delta$ denotes the deviation of the variables from the steady-state operating points, and s is the Laplace complex variable.

For PSS input $u_{PSS\Delta}$, the variables must be used which contain information about oscillations. These variables are electrical power, rotor angle, rotor speed, frequency, terminal voltage, and acceleration torque. The electrical power is selected commonly as the input to the PSS. The output of the PSS, $y_{PSS\Delta}$, is the control signal for the excitation system. A transfer function of a conventional linear PSS is represented as follows:

$$G_{PSS}(s) = \frac{y_{PSS}(s)}{u_{PSS}(s)} = k_{PSS}\left(\frac{sT_1 + 1}{sT_2 + 1}\right)\left(\frac{sT_3 + 1}{sT_4 + 1}\right)\left(\frac{sT_w}{sT_w + 1}\right)G_{aaf}(s) \qquad (20)$$

where k_{PSS} denotes the stabilizer gain [pu]; T_1, T_2, T_3, and T_4 are time constants of the stabilizers lead–lag compensators [s]; T_w is the time constant of the high-pass (washout) filter [s]; and $G_{aaf}(s)$ is the transfer function of the low-pass (antialiasing) filter.

Based on the block diagram in **Figure 20** and the transfer function in (Eq. (6)), the IEEE Association established the IEEE Standard for the PSS studies [11]. The Standard enables the unification of commercial applications of PSS. The Standard sets out four basic types of PSS, which differ mainly with regard to the available input and degree of the transfer function. Most of the commercial PSS are realized on the standardized proposals.

For synthesis of a PSS, knowledge is required of a mathematical model of a synchronous generator with an excitation system. The required model is calculated from the known data of a synchronous generator, or by means of identification. Usage of systematic methods for tuning parameters of conventional PSS assures effective damping for the nominal operating point, though with a significantly decreased damping for some non-nominal operating points. The other disadvantages of these methods are the requirement of the synchronous generator mathematical model's parameters and the time-consuming tuning. Therefore, in practice, the systematic methods are rarely implemented. Hence, neither optimal damping in the nominal operating point nor stable operation is secured in the entire operating range. The implementations of an incorrectly tuned PSS could be harmful. Such PSS are, in practice, often turned off [12].

Due to a mathematical model of a synchronous generator not being available, sophisticated and time-consuming synthesis of the conventional linear PSS, and its proven non-optimum damping in the entire operating range of synchronous generator, advanced control theories are recommended for the PSS implementation.

5. Robust PSS

Among many robust control approaches, the sliding mode control is one of the most interesting. The main advantages of this control are its insensitivity to parameter variations, rejection of disturbances, a decoupling design procedure, and simple implementations by means of power converters [13].

The fundamentals of the sliding mode control theory date back to the late 1950s. Since that time, new research directions emerged, due to the appearance of new

classes of control problems, new mathematical methods, and new prospects of implementation [13–15].

A modification of the sliding mode control based on the decoupling principle will be used for the proposed PSS design. The mathematical model of the controlled plant must be transformed to a regular form:

$$\dot{\mathbf{x}}_{RF1}(t) = \mathbf{A}_{RF11}\mathbf{x}_{RF1}(t) + \mathbf{A}_{RF12}\mathbf{x}_{RF2}(t) \tag{21}$$

$$\dot{\mathbf{x}}_{RF2}(t) = \mathbf{A}_{RF21}\mathbf{x}_{RF1}(t) + \mathbf{A}_{RF22}\mathbf{x}_{RF2}(t) + \mathbf{B}_{RF2}\mathbf{u}_p(t) \tag{22}$$

where $\mathbf{A}_{RFij}$ (i,j = 1,2) and $\mathbf{B}_{RF2}$ are constant matrices of relevant dimensions, $\mathbf{x}_{RF1}(t) \in \mathfrak{R}^{n-m}$ and $\mathbf{x}_{RF2}(t) \in \mathfrak{R}^{m}$ are state-space vectors, and $\mathbf{u}_p(t)$ is a controlled plant input vector. Matrix $\mathbf{B}_{RF2}$ must be nonsingular.

For the PSS design being based on the simplified linearized model of synchronous generator, a state-space vector in regular form $\mathbf{x}_{RF}(t)$, where n = 3 and m = 1, could be selected as

$$\mathbf{x}_{RF}(t) = \begin{bmatrix} \mathbf{x}_{RF1}(t) \\ \mathbf{x}_{RF2}(t) \end{bmatrix} \quad \text{where}: \ \mathbf{x}_{RF1}(t) = \begin{bmatrix} \delta_\Delta(t) \\ \dot{\delta}_\Delta(t) \end{bmatrix} \quad \text{and} \quad \mathbf{x}_{RF2}(t) = \ddot{\delta}_\Delta(t) \tag{23}$$

Sliding mode control for implementation in PSS requires knowledge of all state-space variables of the synchronous generator's regular form model. Measurements of electrical power, rotor speed, and terminal voltage are feasible only at the synchronous generator. For the sliding mode control, the state-space variables for the regular form model need to be calculated from the measured variables. To calculate regular form state-space variables, firstly, variables $\delta_\Delta(t)$ and $E'_{q\Delta}(t)$ can be calculated by inverting (Eq. (19)), such as

$$\begin{bmatrix} \delta_\Delta(t) \\ E'_{q\Delta}(t) \end{bmatrix} = \frac{1}{K_1 K_6 - K_2 K_5} \begin{bmatrix} K_6 & -K_2 \\ -K_5 & K_1 \end{bmatrix} \begin{bmatrix} P_{e\Delta}(t) \\ V_{t\Delta}(t) \end{bmatrix} \tag{24}$$

Finally, state-space variables $\mathbf{x}_{RF1}(t)$ and $\mathbf{x}_{RF2}(t)$ can be calculated with transformation

$$\begin{bmatrix} \delta_\Delta(t) \\ \dot{\delta}_\Delta(t) \\ \ddot{\delta}_\Delta(t) \end{bmatrix} = \begin{bmatrix} 1 & 0 & 0 \\ 0 & \omega_r & 0 \\ -\dfrac{K_1\omega_s}{2H} & -\dfrac{D\omega_s}{2H} & -\dfrac{K_2\omega_s}{2H} \end{bmatrix} \begin{bmatrix} \delta_\Delta(t) \\ \omega_\Delta(t) \\ E'_{q\Delta}(t) \end{bmatrix} \tag{25}$$

In such a way, the state-space variables could be obtained without explicit differentiation.

A sliding surface was selected, such that the rotor's angle deviation and rotor's speed deviation converged exponentially to zero. For this aim, a linear equation of the sliding surface was selected:

$$\mathbf{s}(t) = \mathbf{D}\mathbf{x}_{RF1}(t) + \mathbf{x}_{RF2}(t), \quad \mathbf{s}(t) \in \mathfrak{R}^{m} \tag{26}$$

When the sliding mode appears on manifold $\mathbf{s}(t) = 0$ where $\mathbf{x}_{RF2}(t) = -\mathbf{D}\mathbf{x}_{RF1}(t)$, the system behavior is governed by (n-m)-th-order equation

$$\dot{\mathbf{x}}_{RF1} = (\mathbf{A}_{RF11} - \mathbf{A}_{RF12}\mathbf{D})\mathbf{x}_{RF1} \tag{27}$$

To obtain the required dynamic properties of the control system, we assigned eigenvalues of a closed-loop system with a linear feedback. For the controllable

system described with (Eqs. (21), (22)), there exists matrix **D**, which ensures the desired eigenvalues of the system in (Eq. (27)).

In the first stage of design of the sliding mode, we chose the desired eigenvalues of the system described with (Eq. (27)). From the desired eigenvalues, we determined matrix **D** as the solution to the $(n\text{-}m)$-th-order eigenvalue task. Matrix **D** determines the equation of discontinuous sliding surfaces (Eq. (27)).

The second stage of the design procedure is the selection of the discontinuous control law, such that the sliding mode always arises at manifold $\mathbf{s}(t) = 0$, which is equivalent to the stability of the origin in m-dimensional space $\mathbf{s}(t)$. The dynamics on the $\mathbf{s}(t)$ space are described by the equation

$$\begin{aligned}\dot{\mathbf{s}}(t) &= [\mathbf{D}\mathbf{A}_{\mathrm{RF11}} + \mathbf{A}_{RF21}]\mathbf{x}_{\mathrm{RF1}}(t) + [\mathbf{D}\mathbf{A}_{\mathrm{RF12}} + \mathbf{A}_{RF22}]\mathbf{x}_{\mathrm{RF2}}(t) + \mathbf{B}_{\mathrm{RF2}}\mathbf{u}(t) \\ &= \mathbf{E}\mathbf{x}_{\mathrm{RF}}(t) + \mathbf{B}_{\mathrm{RF2}}\mathbf{u}_{\mathrm{p}}(t)\end{aligned} \tag{28}$$

An appropriate choice of the control law represents the discontinuous control described with

$$\mathbf{u}_{\mathrm{p}}(t) = -\mathrm{g}|\mathbf{x}_{\mathrm{RF}}(t)|\mathbf{B}_{\mathrm{RF2}}^{-1}\,\mathrm{sgn}\,\mathbf{s}(t) \tag{29}$$

where $|\mathbf{x}_{\mathrm{RF}}(t)|$ is the sum of vector $\mathbf{x}_{\mathrm{RF}}(t)$ component moduli and g is the constant.

The selected discontinuous control leads to

$$\dot{\mathbf{s}}(t) = \mathbf{E}\mathbf{x}_{\mathrm{RF}}(t) - \mathrm{g}|\mathbf{x}_{\mathrm{RF}}(t)|\,\mathrm{sgn}\,\mathbf{s}(t) \tag{30}$$

There exists such positive value of g that the functions $\mathbf{s}(t)$ and $\dot{\mathbf{s}}(t)$ have different signs. It means that the sliding mode will occur on a discontinuity surface. The influence of discontinuity of the control signal is reduced by varying the amplitude of the control signal.

6. Adaptive PSS

Many examples with utilization of different adaptive techniques for realization of PSS can be found in publications. The majority of PSS realizations are based on usage of indirect adaptive control, where explicit identification of a mathematical model of a synchronous generator is needed to be carried out [16, 17]. A transparent structure of the adaptive control system with the separated identification algorithm and the control law represents an advantage of indirect adaptive PSS. There are significantly less publications available where usage of direct adaptive control for PSS is presented [18]. The methods of direct adaptive control are more difficult to be utilized for the conventional PSS structure than those for the indirect adaptive control. However, their advantage is in not requiring explicit identification of the SG, and they are, therefore, computationally less demanding. In this article, the developed robust PSS will be compared with direct adaptive PSS which was studied in detail in [2].

The theoretical foundation for the used direct adaptive PSS is represented by a theory of model reference adaptive control for almost strictly positive real plants.

The implemented direct adaptive control is considered for the controlled plant, which is described by

$$\dot{\mathbf{x}}_{\mathrm{p}}(t) = \mathbf{A}_{\mathrm{p}}\mathbf{x}_{\mathrm{p}}(t) + \mathbf{B}_{\mathrm{p}}\mathbf{u}_{\mathrm{p}}(t) \tag{31}$$

$$\mathbf{y}_{\mathrm{p}}(t) = \mathbf{C}_{\mathrm{p}}\mathbf{x}_{\mathrm{p}}(t) \tag{32}$$

where $\mathbf{x}_p(t) \in \mathfrak{R}^n$ is the controlled plant state-space vector, $\mathbf{u}_p(t) \in \mathfrak{R}^m$ is the controlled plant input vector, $\mathbf{y}_p(t) \in \mathfrak{R}^r$ is the controlled plant output vector, and $\mathbf{A}_p$, $\mathbf{B}_p$, and $\mathbf{C}_p$ are the matrices of the appropriate dimensions.

It is assumed that:

• The range of the plant matrices parameters is bounded.

• All possible pairs $\mathbf{A}_p$ and $\mathbf{B}_p$ are controllable and output stabilizable.

• All possible pairs $\mathbf{A}_p$ and $\mathbf{C}_p$ are observable.

The reference model is described by

$$\dot{\mathbf{x}}_m(t) = \mathbf{A}_m \mathbf{x}_m(t) + \mathbf{B}_m \mathbf{u}_m(t) \tag{33}$$

$$\mathbf{y}_m(t) = \mathbf{C}_m \mathbf{x}_m(t) \tag{34}$$

where $\mathbf{x}_m(t)$ is the model state vector, $\mathbf{u}_m(t)$ is the model command vector, $\mathbf{y}_m(t)$ is the model output vector, and $\mathbf{A}_m$, $\mathbf{B}_m$, and $\mathbf{C}_m$ are matrices of appropriate dimensions. The model is assumed to be stable. The dimension of the model state may be less than the dimension of the plant state.

The output tracking error is defined as

$$\mathbf{e}_y(t) = \mathbf{y}_m(t) - \mathbf{y}_p(t) \tag{35}$$

The control $\mathbf{u}_p(t)$ for the plant output vector $\mathbf{y}_p(t)$ to approximate "reasonably well" the output of the reference model $\mathbf{y}_m(t)$ without explicit knowledge of $\mathbf{A}_p$, $\mathbf{B}_p$, and $\mathbf{C}_p$ is generated by the adaptive algorithm:

$$\mathbf{u}_p(t) = \mathbf{K}_e(t)\mathbf{e}_y(t) + \mathbf{K}_x(t)\mathbf{x}_m(t) + \mathbf{K}_u(t)\mathbf{u}_m(t) \tag{36}$$

$$\mathbf{u}_p(t) = \mathbf{K}(t)\mathbf{r}(t) \tag{37}$$

where

$$\mathbf{K}(t) = [\mathbf{K}_e(t), \mathbf{K}_x(t), \mathbf{K}_u(t)] \tag{38}$$

$$\mathbf{r}^T(t) = \left[\mathbf{e}_y^T(t), \mathbf{x}_m^T(t), \mathbf{u}_m^T(t)\right]. \tag{39}$$

The adaptive gains $\mathbf{K}(t)$ are obtained as a combination of the "proportional" and "integral" terms

$$\mathbf{K}(t) = \mathbf{K}_P(t) + \mathbf{K}_I(t) \tag{40}$$

$$\mathbf{K}_P(t) = \mathbf{e}_y(t)\mathbf{r}^T(t)\mathbf{T} \tag{41}$$

$$\dot{\mathbf{K}}_I(t) = \mathbf{e}_y(t)\mathbf{r}^T(t)\overline{\mathbf{T}} - \sigma\mathbf{K}_I(t) \tag{42}$$

where σ term is introduced in order to avoid divergence of the integral gains in the presence of disturbance and $\mathbf{T}$ and $\overline{\mathbf{T}}$ are positive definite and positive semi-definite adaptation coefficient matrices, respectively.

The necessary condition for asymptotic tracking when $\mathbf{u}_m(t)$ is a step command is that the controlled plant is almost strictly positive real (ASPR) [19]. If the controlled plant is not ASPR, the augmenting of the plant with a feedforward

compensator is suggested, such that the augmented plant is ASPR. In this case, the previously described adaptive controller may be utilized.

For the non-ASPR plant described by the transfer matrix

$$\mathbf{G}_\mathrm{p}(s) = \mathbf{C}_\mathrm{p}(s\mathbf{I} - \mathbf{A}_\mathrm{p})^{-1}\mathbf{B}_\mathrm{p} \tag{43}$$

the feedforward compensator is defined by the strictly proper transfer function matrix $\mathbf{G}_\mathrm{ff}(s)$ with the realization

$$\dot{\mathbf{s}}_\mathrm{p}(t) = \mathbf{A}_\mathrm{s}\mathbf{s}_\mathrm{p}(t) + \mathbf{B}_\mathrm{s}\mathbf{u}_\mathrm{p}(t) \tag{44}$$

$$\mathbf{r}_\mathrm{p}(t) = \mathbf{D}_\mathrm{s}\mathbf{s}_\mathrm{p}(t) \tag{45}$$

Instead of the plant output $\mathbf{y}_\mathrm{p}(t)$, augmented output $\mathbf{z}_\mathrm{p}(t)$ is to be controlled:

$$\mathbf{z}_\mathrm{p}(t) = \mathbf{y}_\mathrm{p}(t) + \mathbf{r}_\mathrm{p}(t) \tag{46}$$

The augmented system is defined as

$$\mathbf{G}_\mathrm{a}(s) = \mathbf{G}_\mathrm{p}(s) + \mathbf{G}_\mathrm{ff}(s) \tag{47}$$

Feedforward compensator $\mathbf{G}_\mathrm{ff}(s)$ is an inverse of a (fictitious) stabilizing controller for the plant and must be selected such that the resulting relative degree of augmented plant $\mathbf{G}_\mathrm{a}(s)$ is indeed 1. For example, if SISO plant $\mathbf{G}_\mathrm{p}(s)$ is stabilizable by a PD controller, one can use its inverse in a manner that is just a simple first-order low-pass filter.

7. Results

The effectiveness of the proposed sliding mode PSS and direct adaptive PSS was tested with the simulations of the seventh-order nonlinear model of the synchronous generator in the entire operating range, numerically, as well as experimentally, in the laboratory.

7.1 Robust PSS

A block diagram of the sliding mode PSS is shown in **Figure 21**.

A sliding mode controller requires measurements of three synchronous generator's quantities: electrical power, rotor speed, and terminal voltage. Input filters are low-pass filters to eliminate the measured noise. From these measured variables, the state-space variables for the regular form model are calculated by means of state transformation. State transformation is carried out by Eqs. (24) and (25). The obtained regular form state-space variables are used in the control law described with Eqs. (26) and (29). The output of the discontinuous control law is conducted in the limiter. Hard type saturation of the PSS output was utilized, with a limited value of ±35% of the value of a nominal rotor excitation voltage. The set value represents a limitation in a real excitation system.

For a synchronous generator with the data listed in Section 3, we selected desired eigenvalues $\lambda_{1,2} = -2$ for the system in (Eq. (27)). The following control law parameters were calculated [2]:

$$\mathbf{D} = \begin{bmatrix} 4 & 4 \end{bmatrix} \quad \mathbf{B}_\mathrm{RF2}^{-1} = -0.06 \quad g = 350 \tag{48}$$

ROBUST PSS

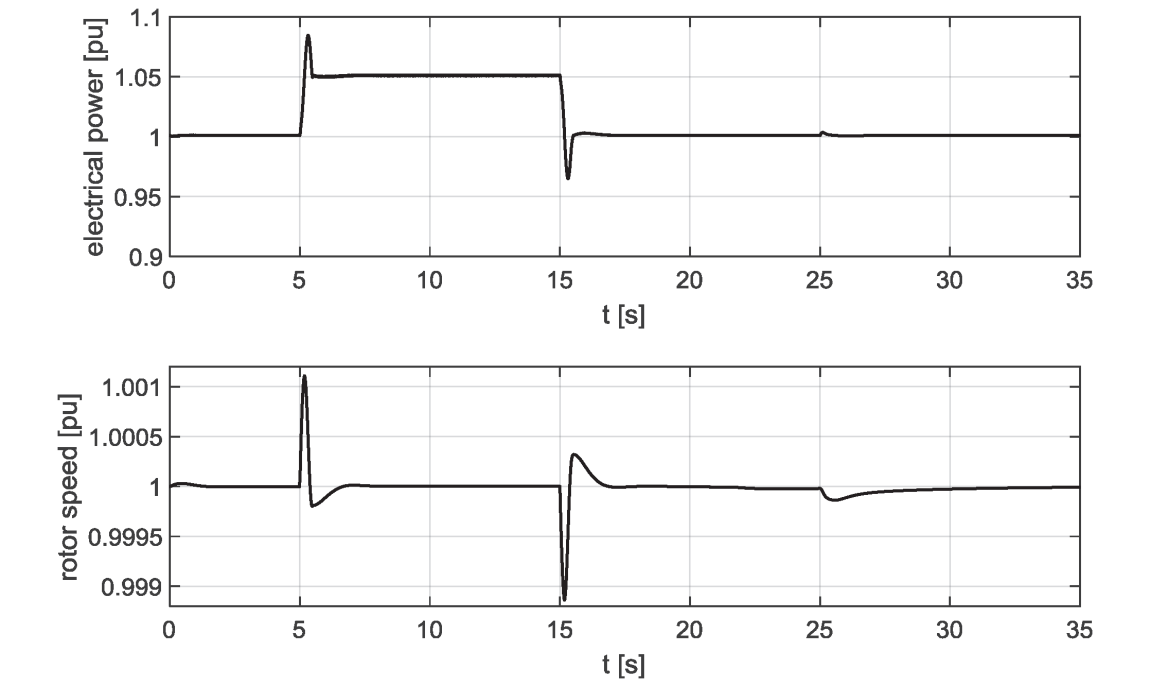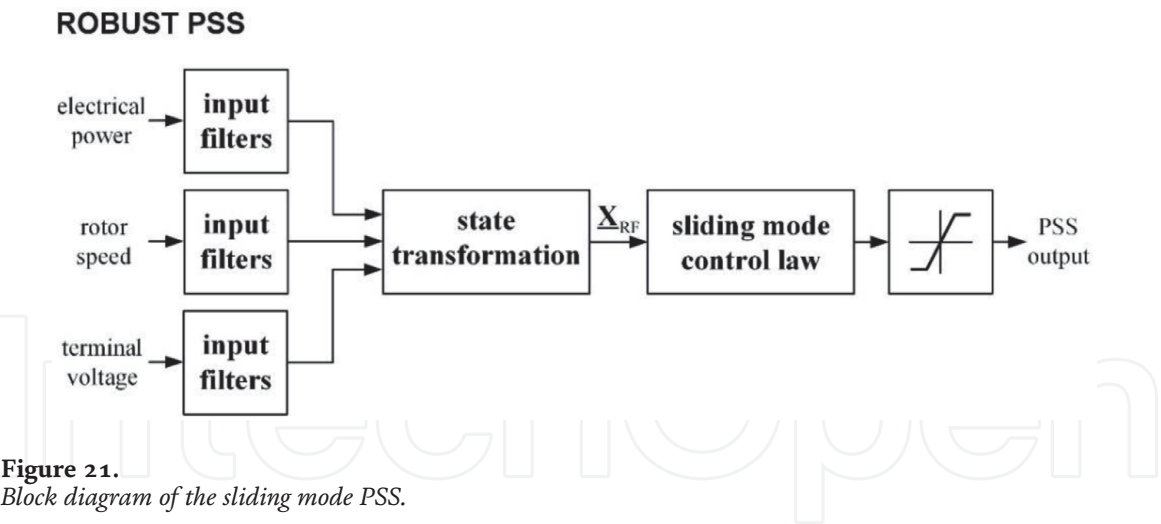**Figure 21.**
Block diagram of the sliding mode PSS.

Figure 22.
Electrical power $P_e(t)$ [pu] and rotor speed $\omega(t)$ [pu] at nominal operating point P = 1.0 [pu] and Q = 0.62 [pu], with robust PSS.
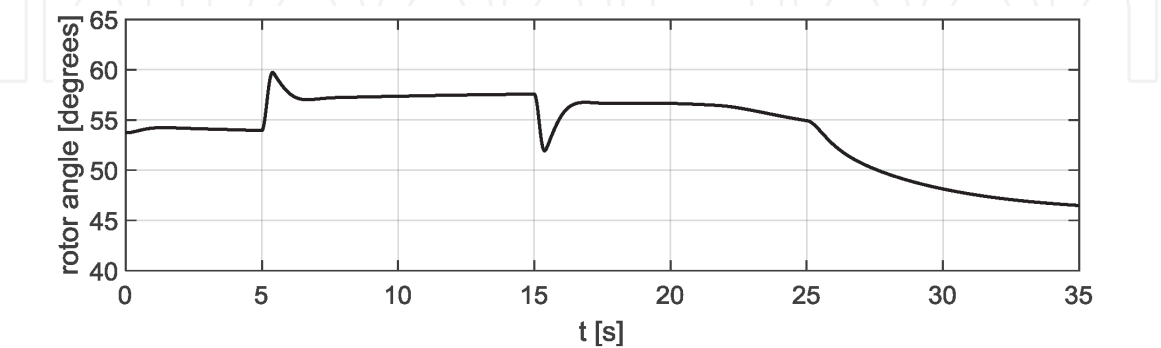

Figure 23.
Rotor angle $\delta(t)$ [pu] at nominal operating point P = 1.0 [pu] and Q = 0.62 [pu], with robust PSS.

7.1.1 Nominal operating point

Figures 22–24 show the responses of the seventh-order nonlinear model of the considered 160 MVA synchronous generator equipped with an excitation system

and robust PSS to the step changes of the mechanical torque and the field excitation voltage, as shown in **Figure 11**. The synchronous generator operates in in the vicinity of the nominal operating point. **Figures 22** and **23** show the generated electrical power, rotor speed, and rotor angle at nominal operating point P = 1.0 [pu] and Q = 0.62 [pu].

Figure 24 shows the excitation voltage produced by a robust PSS at operating point P = 1.0 [pu] and Q = 0.62 [pu]. The limits of the limiters are seen clearly.

7.1.2 Influence of load disturbance

During the operation in the entire operating range, the dynamics of the synchronous generator vary significantly. The sliding mode controller with the calculated parameters was stable and robust and displayed the effective damping in all operating conditions. The theoretical analysis of the invariance of the proposed control system to the disturbances and the variation of the plant parameter are described in detail in [20].

In this work, the results of the two most extreme operating points are presented (the same operating points as described in Section 3.2):

- P = 1.0 [pu] and Q = 0.1 [pu]: This is a stable operation point with heavily damped oscillations.

- P = 0.1 [pu] and Q = 1.0 [pu]: This is the critical operating point with weakly damped oscillations.

Figure 25 shows the generated electrical power and rotor speed at operating point P = 1.0 [pu] and Q = 0.1 [pu], and **Figure 26** shows both quantities at operating point P = 0.1 [pu] and Q = 1.0 [pu].

7.1.3 Influence of parameter deviations

To analyze the impact of parameter variations on the damping efficiency of the proposed control systems, both control systems were tested at different operating points for synchronous generators of different types and nominal powers. In this work, the results are presented for a synchronous generator with nominal power 555 MVA. The data of the considered synchronous generator are shown in **Table 10** [4].

The linearization coefficients for nominal operating point (P_N = 1 [pu], cos φ_N = 0.9) and eigenvalues of the Heffron-Phillips model (λ_1, λ_2, λ_3) are presented in **Table 11**.

The transient response of the noncontrolled synchronous generator with data in **Table 10** and nominal operating point data in **Table 11** are shown in
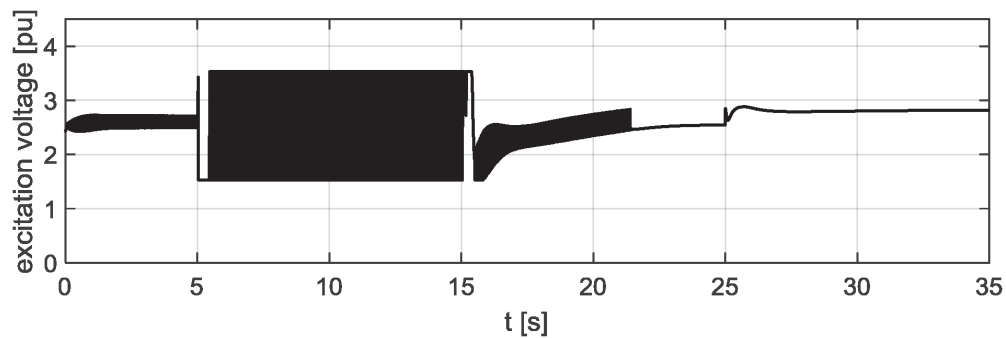

Figure 24.
Excitation voltage $E_{FD}(t)$ *[pu] at nominal operating point P = 1.0 [pu] and Q = 0.62 [pu], with robust PSS.*
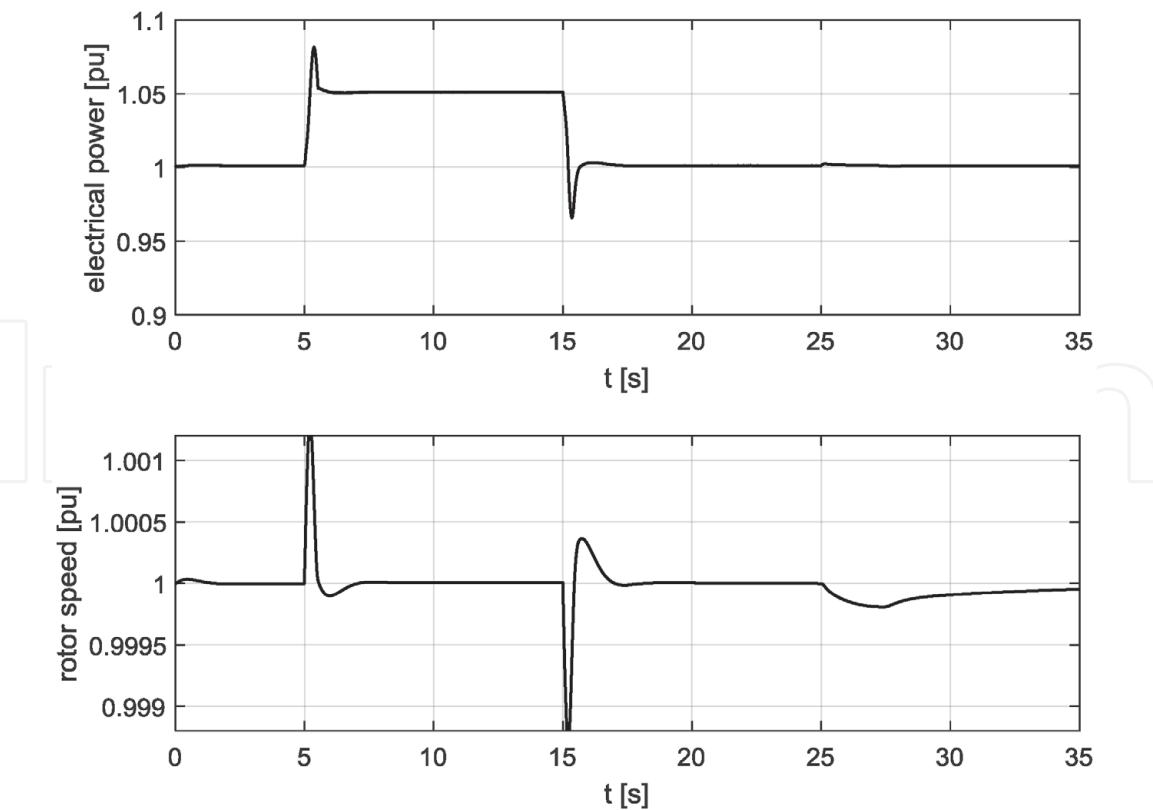
Figure 25.
Electrical power $P_e(t)$ *[pu] and rotor speed* $\omega(t)$ *[pu] at operating point P = 1.0 [pu] and Q = 0.1 [pu], with robust PSS.*
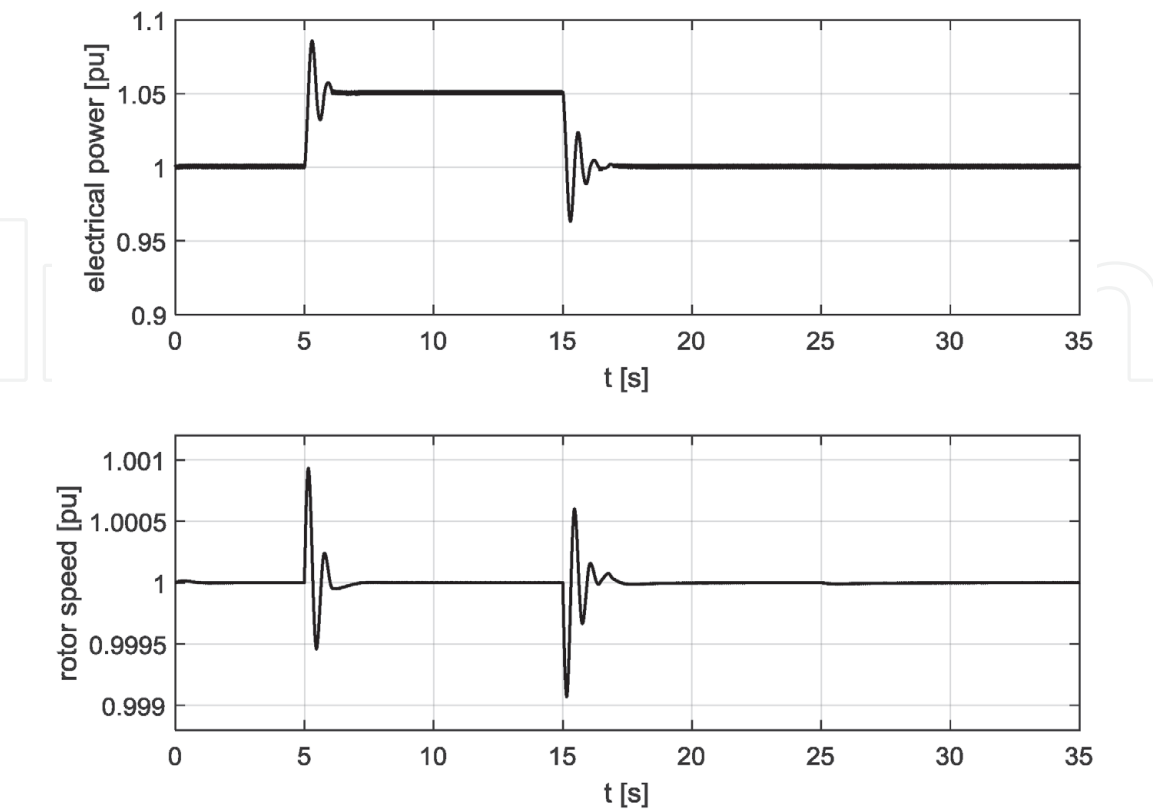

Figure 26.
Electrical power $P_e(t)$ *[pu] and rotor speed* $\omega(t)$ *[pu] at operating point P = 0.1 [pu] and Q = 1.0 [pu], with robust PSS.*

Figures 27 and **28**. Step changes are simulated in both generators' inputs. **Figure 27** shows the simulated trajectory of the turbine mechanical torque and rotor excitation voltage. Step changes are selected as the worst case in order to maximize the excitation of oscillations.

Figure 28 shows the response of the generated electrical power and rotor speed on the inputs' trajectories shown in **Figure 27**.

S_N = 555 [MVA]	V_N = 24 [kV]	$\cos \varphi_N$ = 0.90
ω_s = 377 [rad s^{-1}]		
T'_{d0} = 8.0 [pu]	H = 3.52 [s]	D = 2.0 [pu]
R_e = 0.02 [pu]	L_e = 0.4 [pu]	V_{IB} = 1.0 [pu]
R_s = 0.0030 [pu]	R_F = 0.0006 [pu]	x'_d = 0.300 [pu]
L_d = 1.810 [pu]	L_q = 1.760 [pu]	L_F = 0.165 [pu]
L_D = 0.171 [pu]	L_Q = 0.084 [pu]	L_{AD} = 1.660 [pu]
l_d = 0.150 [pu]	l_q = 0.150 [pu]	L_{AQ} = 1.610 [pu]

Table 10.
Data of the 555 MVA synchronous generator used for the analysis of the impact of parameter variations on the damping efficiency [4].

P_N = 1.0 [pu]	Q_N = 0.48 [pu]	$\cos \varphi_N$ = 0.90
K_1 = 1.3306	K_2 = 1.2988	K_3 = 0.3168
K_4 = 1.8578	K_5 = −0.0107	K_6 = 0.4545
λ_1 = −0.2554 + 8.4389i	λ_2 = −0.2554 - 8.4389i	λ_3 = −-0.1678

Table 11.
Linearization parameters and eigenvalues of the Heffron-Phillips model at the nominal operating point of the 555 MVA synchronous generator.
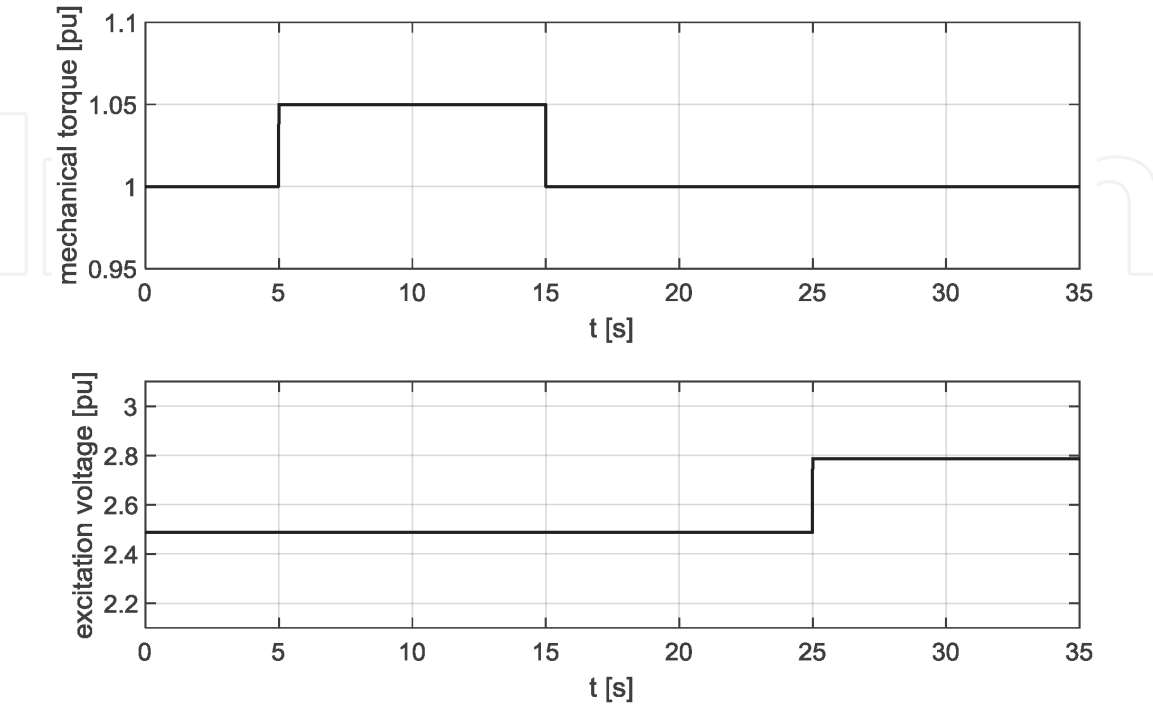

Figure 27.
The 555 MVA synchronous generator inputs' trajectories: Mechanical torque $T_m(t)$ [pu] and rotor excitation voltage $E_{fd}(t)$ [pu], nominal operating point P = 1.0 [pu] and Q = 0.48 [pu].
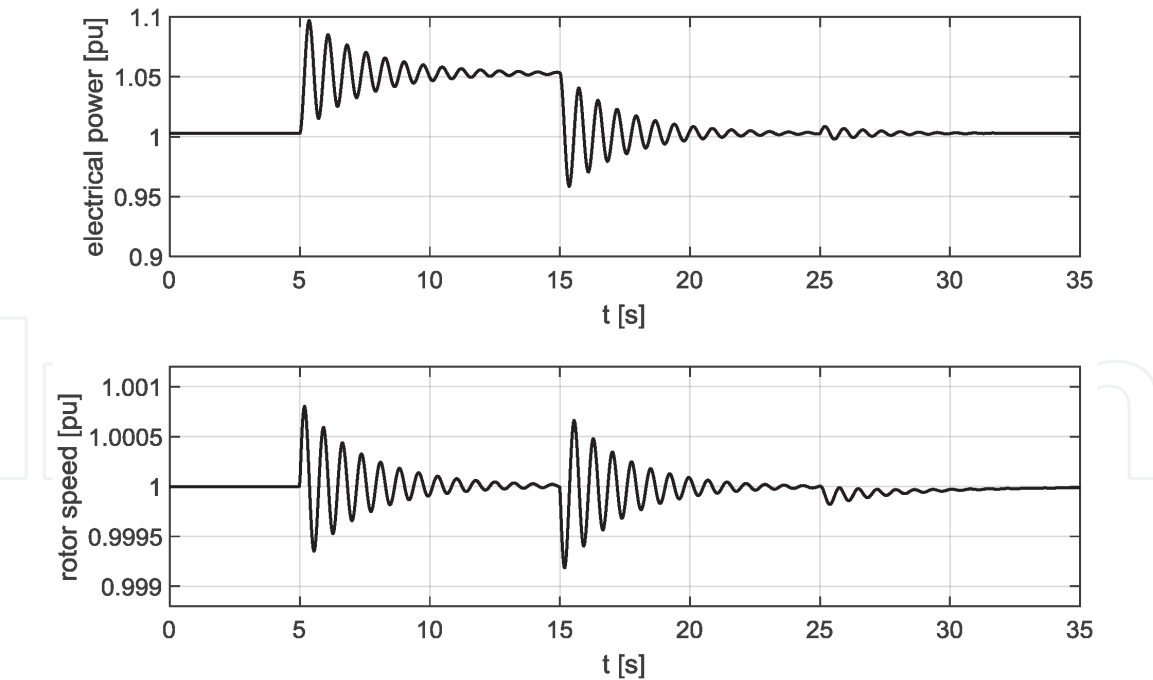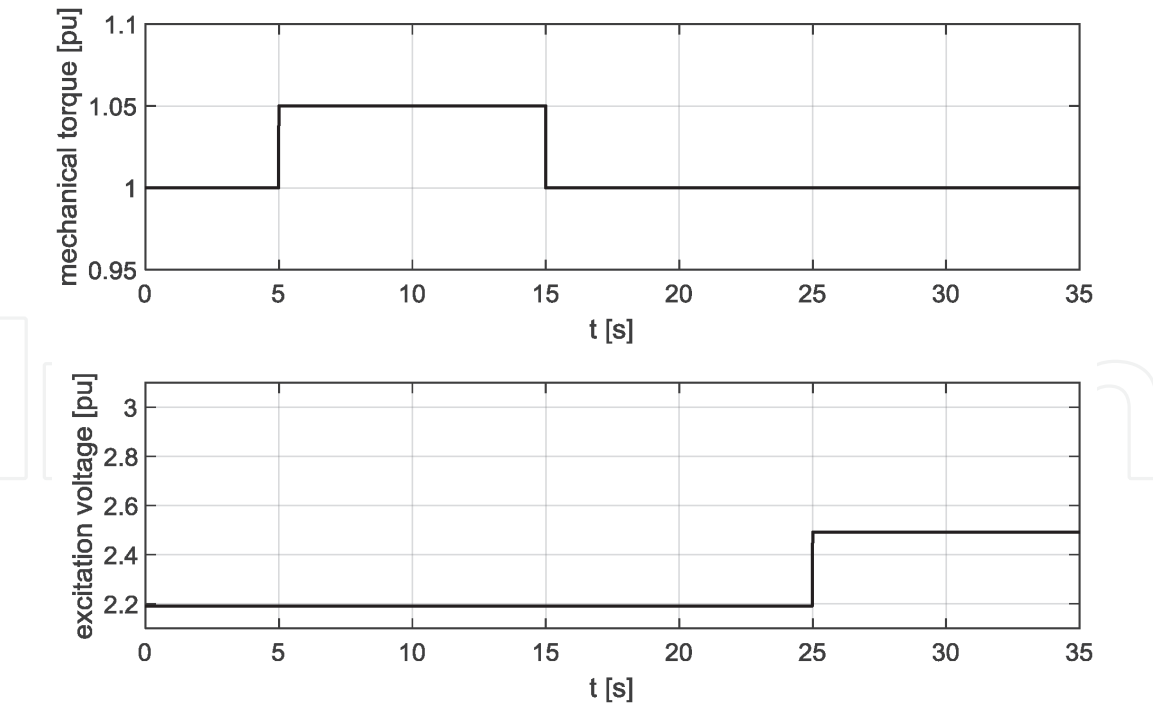
Figure 28.
The 555 MVA synchronous generator outputs' trajectories: Rotor speed ω(t) [pu] and rotor angle δ(t) [degrees], nominal operating point P = 1.0 [pu] and Q = 0.48 [pu], without PSS.

P_N = 1.0 [pu]	Q_N = 0.1 [pu]	$\cos \varphi_N$ = 0.995
K_1 = 1.1387	K_2 = 1.4710	K_3 = 0.3168
K_4 = 2.1296	K_5 = −0.1069	K_6 = 0.3281
λ_1 = −0.3140 + 7.8075i	λ_2 = −0.3140 - 7.8075i	λ_3 = −0.0506

Table 12.
Performance in linearization parameters and eigenvalues of the Heffron-Phillips model in operating point P = 1.0 [pu] and Q = 0.1 [pu] of the 555 MVA synchronous generator.

P_N = 0.1 [pu]	Q_N = 1.0 [pu]	$\cos \varphi_N$ = 0.099
K_1 = 1.2340	K_2 = 0.1533	K_3 = 0.3168
K_4 = 0.1204	K_5 = 0.0167	K_6 = 0.5720
λ_1 = −0.1430 - 8.1276i	λ_2 = −0.1430 + 8.1276i	λ_3 = −0.3927

Table 13.
Linearization parameters and eigenvalues of the Heffron-Phillips model at operating point P = 0.1 [pu] and Q = 1.0 [pu] of the 555 MVA synchronous generator.

The results are presented of the robust control at two operating points:

- *P* = 1.0 [pu] and *Q* = 0.1 [pu]: The linearization coefficients and eigenvalues of the Heffron-Phillips model (λ_1, λ_2, λ_3) are presented in **Table 12**, the step changes of the mechanical torque and the field excitation voltage are shown in **Figure 29**, and the generated electrical power and rotor speed are shown in **Figure 30**.

- *P* = 0.1 [pu] and *Q* = 1.0 [pu]: The linearization coefficients and eigenvalues of the Heffron-Phillips model (λ_1, λ_2, λ_3) are presented in **Table 13**, the step

Figure 29.
The 555 MVA synchronous generator inputs' trajectories: Mechanical torque T_m(t) [pu] and rotor excitation voltage E_{fd}(t) [pu], operating point P = 1.0 [pu] and Q = 0.1 [pu].
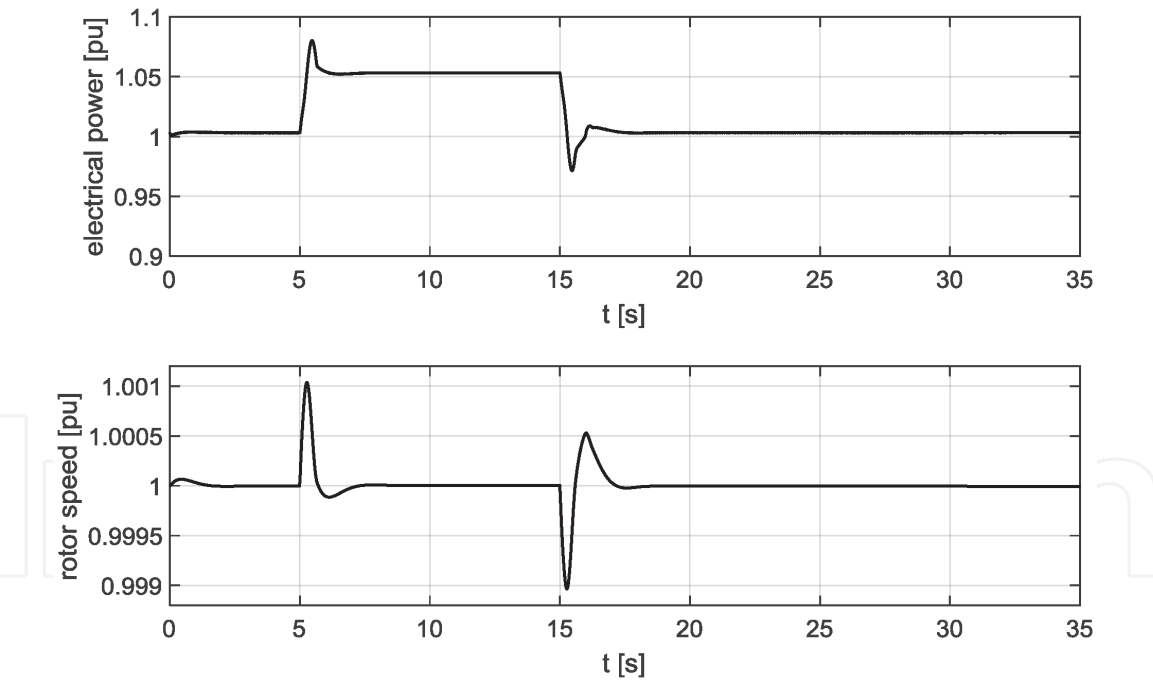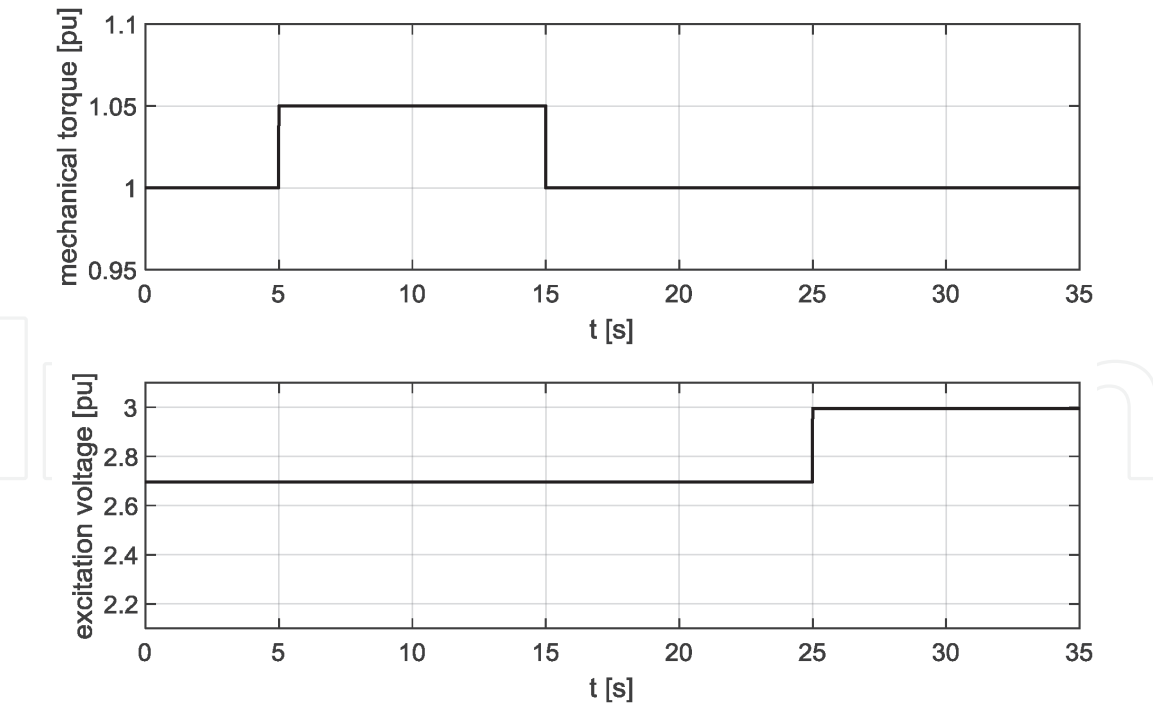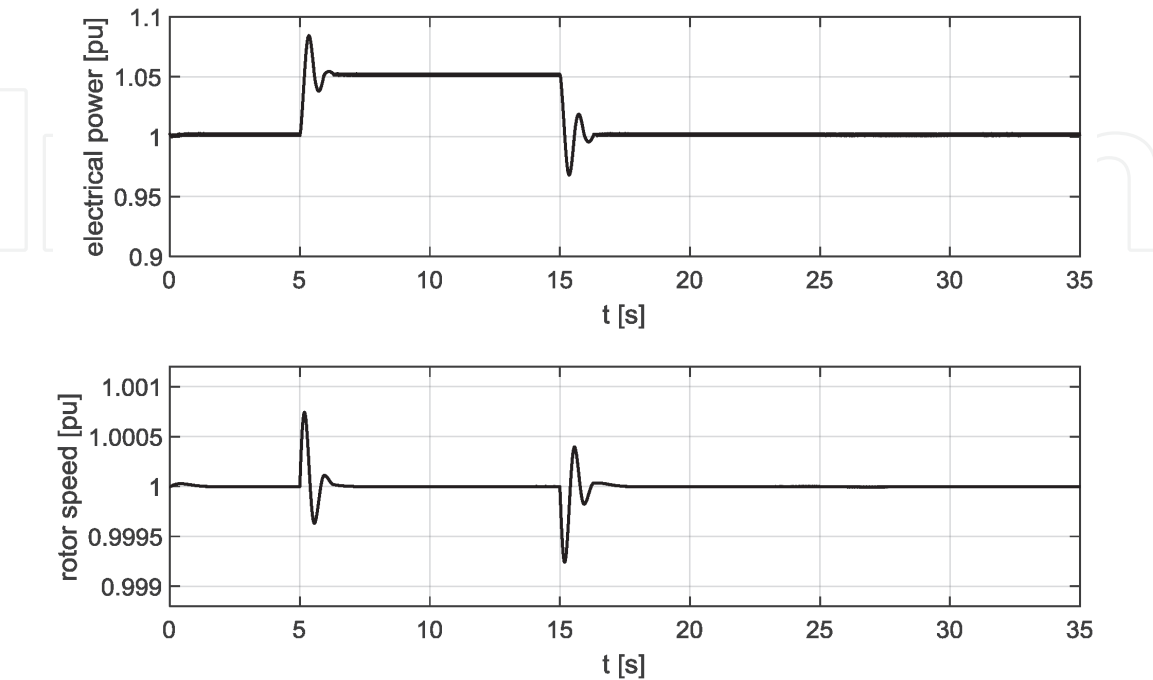

Figure 30.
The 555 MVA synchronous generator's electrical power P_e(t) [pu] and rotor speed ω(t) [pu] at nominal operating point P = 1.0 [pu] and Q = 0.1 [pu], with robust PSS.

changes of the mechanical torque and the field excitation voltage are shown in **Figure 31**, and the generated electrical power and rotor speed are shown in **Figure 32**.

Figure 25 shows the generated electrical power and rotor speed at heavily damped operating point *P* = 1.0 [pu] and *Q* = 0.1 [pu], and **Figure 26** shows both quantities at weakly damped operating point *P* = 0.1 [pu] and *Q* = 1.0 [pu].

Figure 31.
The 555 MVA synchronous generator inputs' trajectories: Mechanical torque T_m(t) [pu] and rotor excitation voltage E_{fd}(t) [pu], operating point P = 0.1 [pu] and Q = 1.0 [pu].

7.2 Adaptive PSS

The proposed direct adaptive controller guarantees stability of any controlled plant that satisfies ASPR conditions. A synchronous generator with automatic voltage system does not satisfy the necessary ASPR conditions. Augmenting of the plant with a parallel feedforward compensator must be carried out to assure stable operation of the entire adaptive control system. The augmentation is performed such

Figure 32.
The 555 MVA synchronous generator's electrical power P_e(t) [pu] and rotor speed ω(t) [pu] at nominal operating point P = 0.1 [pu] and Q = 1.0 [pu], with robust PSS.

that the augmented plant fulfills ASPR conditions. The requirement is satisfied in the majority of cases with the introduction of a feedforward compensator $G_{ff}(s)$, which is connected in parallel to the basic controlled plant. The suitable feedforward stabilizer represents a first-order low-pass filter with feedforward compensator gain k_{ff} and feedforward compensator time constant T_{ff} [18].

A block diagram of the direct adaptive PSS is presented in **Figure 33**.

The benefit of the control diagram shown in **Figure 33**, if compared to other adaptive structures, is a very simple realization of the adaptation mechanism. The presented direct adaptive PSS is essentially simplified; namely, a reference model is not required because of the constant (zero) command signal.

The reference terminal voltage $V_{t,ref}$ and the mechanical torque T_m variables represent the main disturbances which affect the synchronous generator's dynamics. The variations of the synchronous generator loading can be treated as controlled plant parameters' perturbations. The washout block (input filters) serves as a high-pass filter, with the time constant T_w high enough to allow signals associated with oscillations in generator active power P_e to pass unchanged. Without it, steady changes in power would modify the terminal voltage. It allows the PSS to respond only to changes in generator active power. From the viewpoint of the washout function, the value of T_w is not critical and may be in the range of 1–20 s. The main consideration is that it would be long enough to pass stabilizing signals unchanged at the frequencies of interest. Direct adaptive control law is represented with (Eqs. (35)–(42)). The necessary feedforward compensator is described with Eqs. (44) and (45). The same model of the actuator saturation as in Section 7.1.1 was included in the simulations.

The parameters of the adaptation mechanism for the considered linearized controlled plant are determined with the rules described in [2], such as

$$\mathbf{T} = 0.1 \cdot 10^3 \quad \overline{\mathbf{T}} = 200 \cdot 10^3 \quad \sigma = 50 \cdot 10^{-3} \quad k_{ff} = 1 \cdot 10^{-3} \quad T_{ff} = 1 \cdot 10^{-3}$$

$$(49)$$

7.2.1 Nominal operating point

Figures 34–36 show the responses of the seventh-order nonlinear model of the considered 160 MVA synchronous generator equipped with an excitation system and adaptive PSS to the step changes of the mechanical torque and the field excitation voltage, as shown in **Figure 11**. **Figures 34** and **35** show the generated electrical power, rotor speed, and rotor angle at nominal operating point P = 1.0 [pu] and Q = 0.62 [pu].

Figure 36 shows the excitation voltage produced by an adaptive PSS at nominal operating point P = 1.0 [pu] and Q = 0.62 [pu].

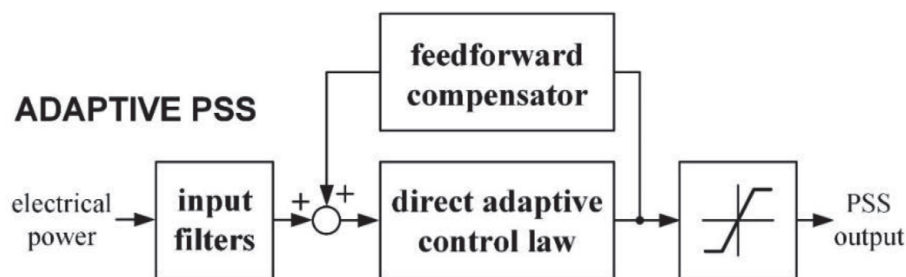**Figures 34–36** are directly comparable with **Figures 22–25**.

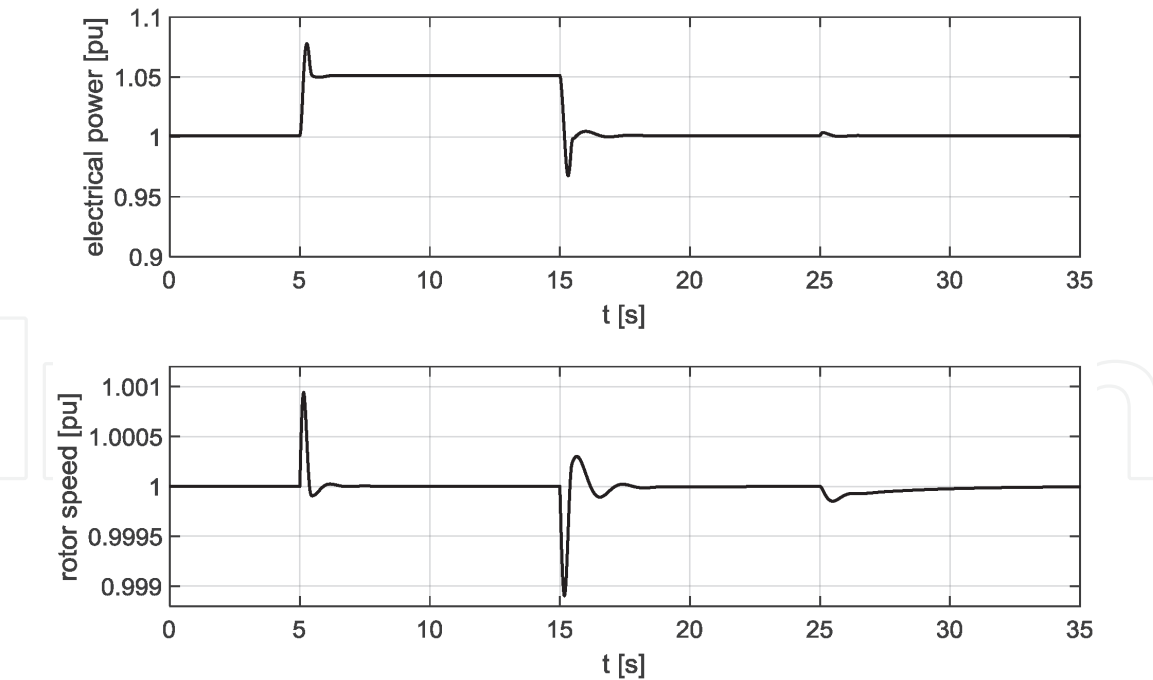**Figure 33.**
Block diagram of the direct adaptive PSS.

Figure 34.
Electrical power $P_e(t)$ *[pu] and rotor speed* $\omega(t)$ *[pu] at operating point P = 1.0 [pu] and Q = 0.62 [pu], with adaptive PSS.*
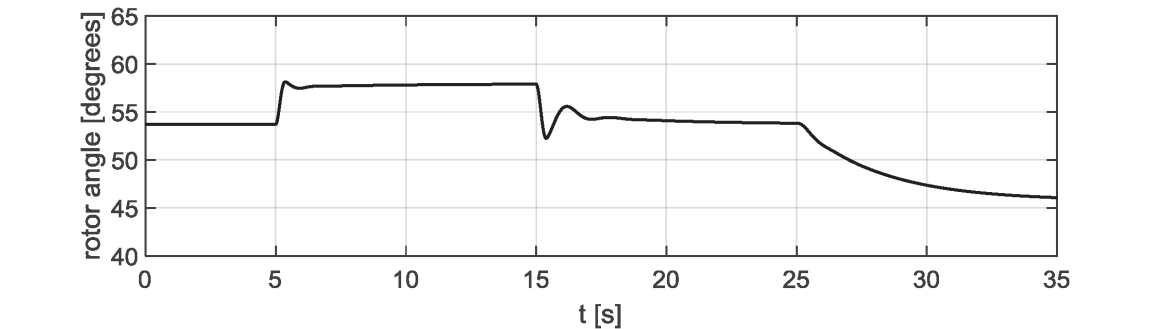

Figure 35.
Rotor angle $\delta(t)$ *[pu] at nominal operating point P = 1.0 [pu] and Q = 0.62 [pu], with adaptive PSS.*
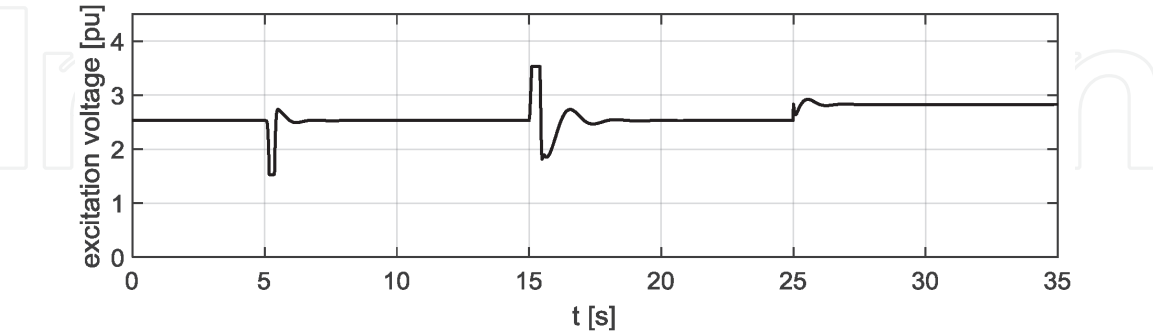

Figure 36.
Excitation voltage $E_{FD}(t)$ *[pu] at nominal operating point P = 1.0 [pu] and Q = 0.62 [pu], with adaptive PSS.*

7.2.2 Influence of load disturbance

The results of the two most extreme operating points are presented (the same as in Sections 3.2 and 7.1.2):

- *P* = 1.0 [pu] and *Q* = 0.1 [pu]: The generated electrical power and rotor speed are shown in **Figure 37**.
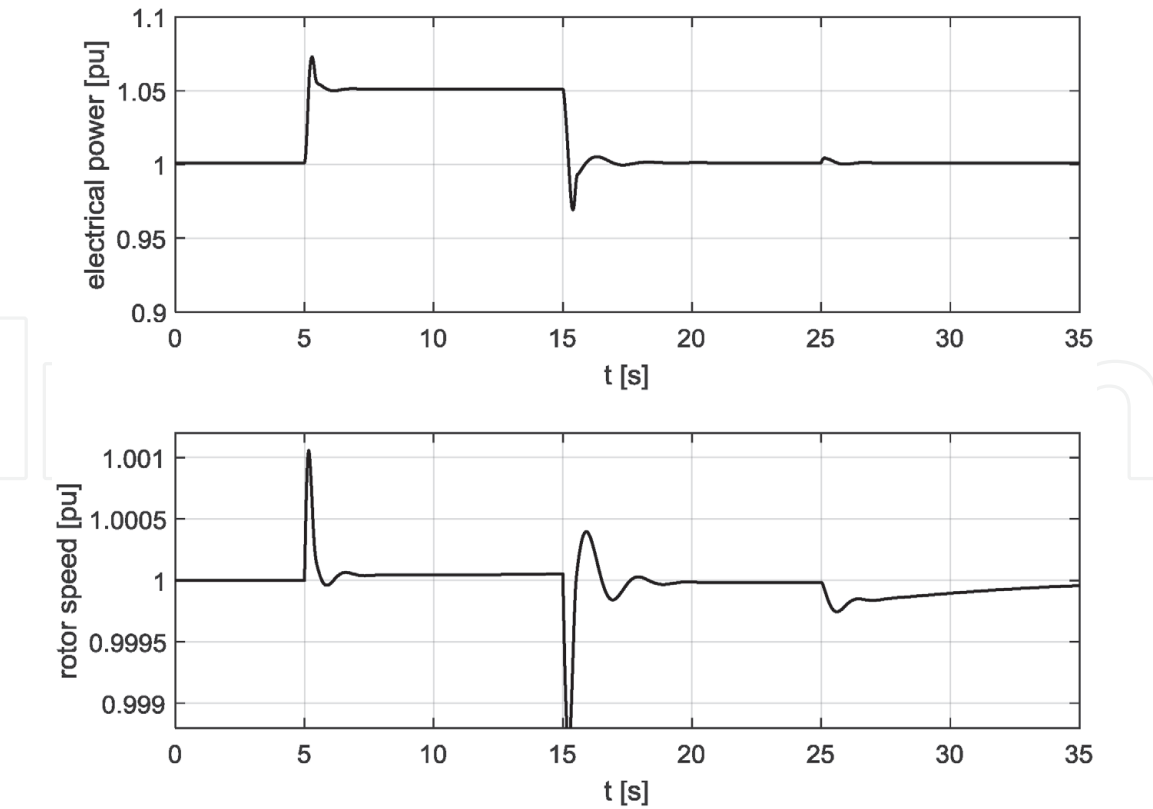
Figure 37.
Electrical power P$_e$(t) [pu] and rotor speed ω(t) [pu] at operating point P = 1.0 [pu] and Q = 0.1 [pu], with adaptive PSS.
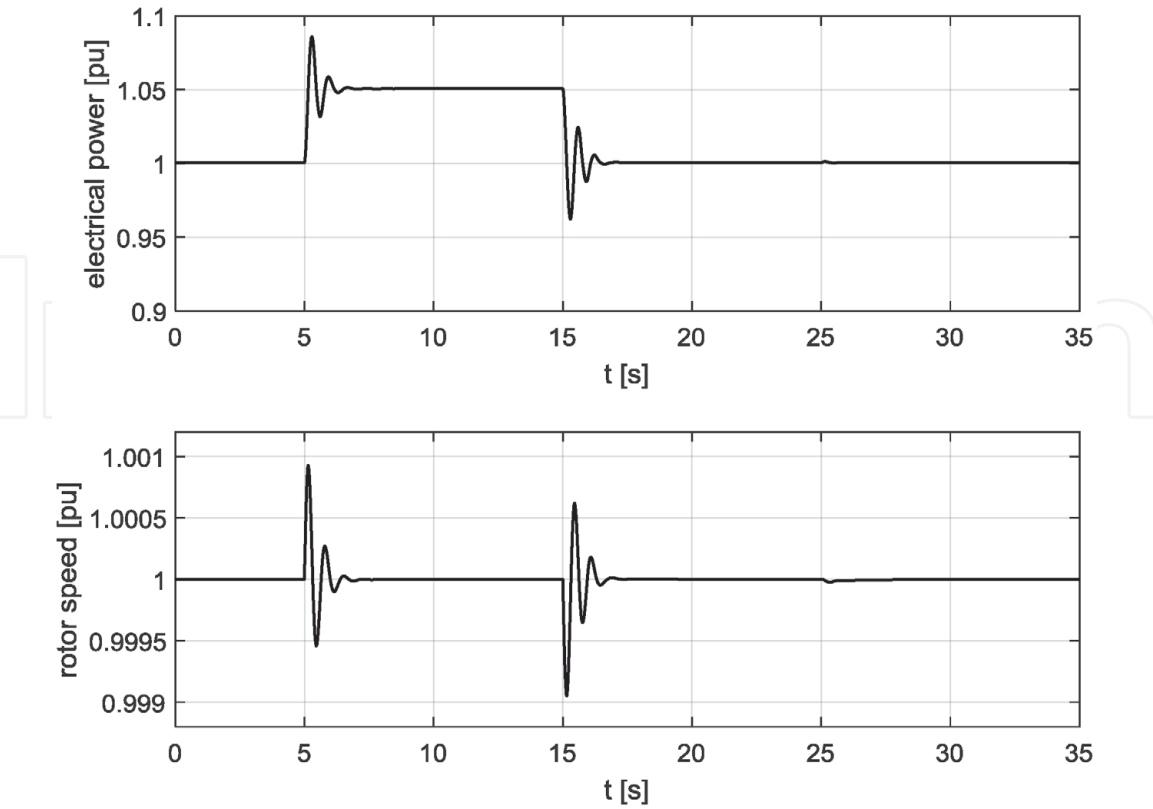

Figure 38.
Electrical power P$_e$(t) [pu] and rotor speed ω(t) [pu] at operating point P = 0.1 [pu] and Q = 1.0 [pu], with adaptive PSS.

- *P* = 0.1 [pu] and *Q* = 1.0 [pu]: The generated electrical power and rotor speed are shown in **Figure 38**.

7.2.3 Influence of parameter deviations

The effectiveness of the adaptive PSS for oscillation damping in the presence of parameter deviations is shown with a test on the 555 MVA synchronous generator,
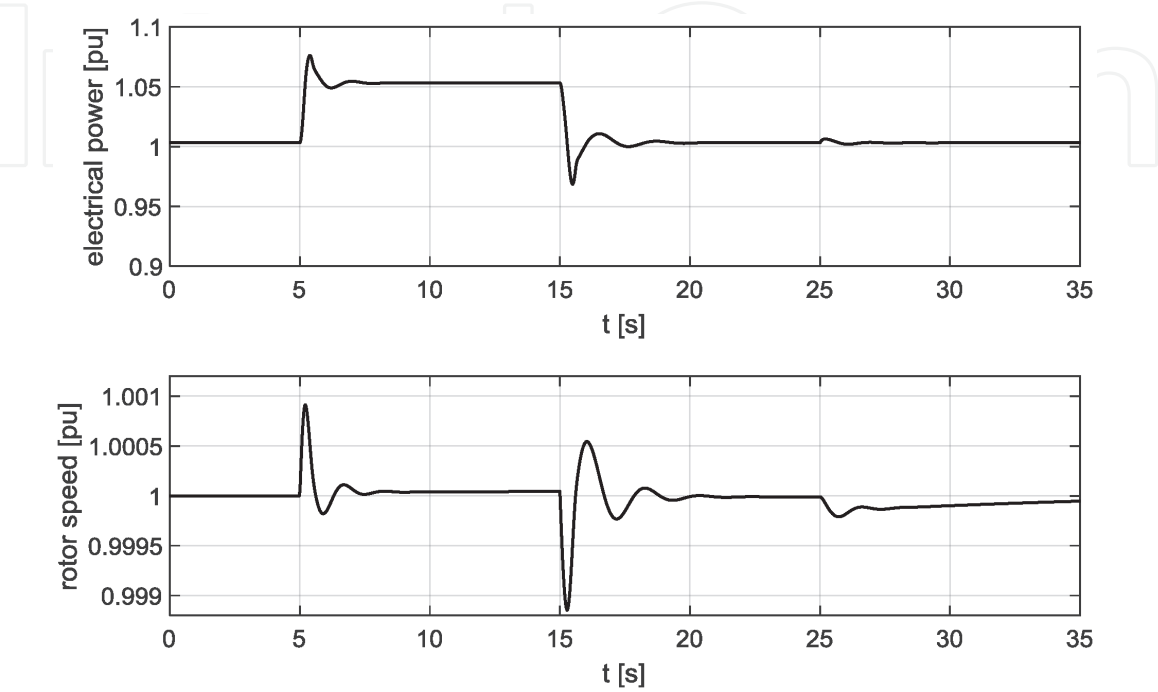
Figure 39.
The 555 MVA synchronous generator's electrical power $P_e(t)$ *[pu] and rotor speed* $\omega(t)$ *[pu] at operating point P = 1.0 [pu] and Q = 0.1 [pu], with adaptive PSS.*
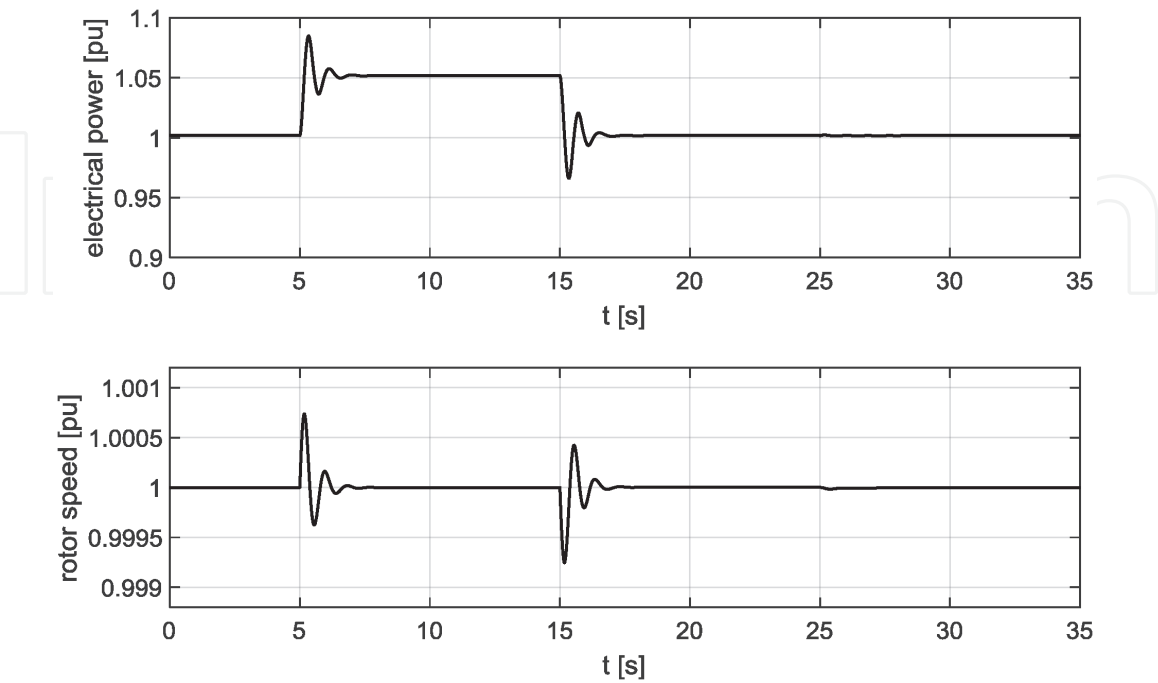
Figure 40.
The 555 MVA synchronous generator's electrical power $P_e(t)$ *[pu] and rotor speed* $\omega(t)$ *[pu] at operating point P = 0.1 [pu] and Q = 1.0 [pu], with adaptive PSS.*

as in Section 7.1.3. **Figure 39** shows the generated electrical power and rotor speed at operating point P = 1.0 [pu] and Q = 0.1 [pu], and **Figure 40** shows both quantities at operating point P = 0.1 [pu] and Q = 1.0 [pu].

7.3 Assessment of the presented power system stabilizers

From the results presented in Sections 7.1 and 7.2 presented in **Figures 22–32** and **34–40**, it is seen clearly that robust and adaptive PSS improve the damping of oscillations of the synchronous generators significantly (shorter time of oscillations, smaller overshoot, and better damping). The numerical assessment was done for better insight into the effectiveness of both control algorithms. The integral square root performance index of rotor speed oscillation ($\int \omega^2 dt$) was introduced for more objective numerical evaluation of the proposed control approaches. The time responses shown in **Figures 13, 16, 19, 22, 25, 26, 34, 37,** and **38** were considered

Synchronous generator with nominal power S_N = 160 [MVA]					
P [pu]	Q [pu]	$\cos \varphi$	Performance index		
			Without PSS	Robust PSS	Adaptive PSS
1.0	0.1	0.995	$1.98 \; 10^{-6}$	$0.96 \; 10^{-6}$	$0.91 \; 10^{-6}$
1.0	0.62	0.85	$0.99 \; 10^{-6}$	$0.56 \; 10^{-6}$	$0.44 \; 10^{-6}$
0.1	1.0	0.099	$0.56 \; 10^{-6}$	$0.41 \; 10^{-6}$	$0.42 \; 10^{-6}$

Table 14.
Integral square root performance index of rotor speed oscillation of the 160 MVA synchronous generator without PSS, with robust PSS, or with adaptive PSS at different operating points.

Synchronous generator with nominal power S_N = 160 [MVA]				
P [pu]	Q [pu]	$\cos \varphi$	Improvement of performance index regarding the case without PSS [%]	
			Robust PSS	Adaptive PSS
1.0	0.1	0.995	51 [%]	54 [%]
1.0	0.62	0.85	43 [%]	55 [%]
0.1	1.0	0.099	26 [%]	25 [%]

Table 15.
The improvements of the integral square root performance index of rotor speed oscillation of the 160 MVA synchronous generator at different operating points following the use of robust or adaptive PSS.

Synchronous generator with nominal power S_N = 555 [MVA]					
P [pu]	Q [pu]	$\cos \varphi$	Performance index		
			Without PSS	Robust PSS	Adaptive PSS
1.0	0.1	0.995	$1.73 \; 10^{-6}$	$0.76 \; 10^{-6}$	$0.92 \; 10^{-6}$
1.0	0.62	0.85	$0.89 \; 10^{-6}$	$0.51 \; 10^{-6}$	$0.47 \; 10^{-6}$
0.1	1.0	0.099	$0.33 \; 10^{-6}$	$0.28 \; 10^{-6}$	$0.28 \; 10^{-6}$

Table 16.
Integral square root performance index of rotor speed oscillation of the 555 MVA synchronous generator without PSS, with robust PSS, or with adaptive PSS at different operating points.

Synchronous generator with nominal power S_N = 555 [MVA]				
P [pu]	Q [pu]	$\cos \varphi$	Improvement of performance index regarding the case without PSS [%]	
			Robust PSS	Adaptive PSS
1.0	0.1	0.995	56 [%]	47 [%]
1.0	0.62	0.85	43 [%]	47 [%]
0.1	1.0	0.099	15 [%]	15 [%]

Table 17.
The improvements of the integral square root performance index of rotor speed oscillation of the 555 MVA synchronous generator at different operating points following the use of robust or adaptive PSS.

for a synchronous generator with nominal power 160 MVA. The calculated performance indexes are shown in **Table 14**. The improvements of the performance index by means of proposed control systems regarding the noncontrolled synchronous generator are presented in **Table 15**.

The time responses shown in **Figures 28, 30, 32, 39**, and **40** were considered for a synchronous generator with nominal power 555 MVA. The calculated performance indexes of the synchronous generator without PSS, with robust PSS, or with adaptive PSS are shown in **Table 16**. The improvements of the performance index by means of proposed control systems regarding the noncontrolled synchronous generator are presented in **Table 17**.

From the obtained numerical results, it is obvious that the proposed robust and adaptive PSS assure significant damping improvement in the entire operating range. The effectiveness of both proposed stabilizers are similar. They depend on the type of generator, largeness of the generator, operating point (loading), etc. In general, we can conclude that, according to the introduced performance index, their improvement is in the range of 10–60 [%].

8. Conclusion

Changes in construction of synchronous generators and the introduction of additional control systems into power systems have led to significant increase of oscillations in power systems and related stability problems. Conventional linear power system stabilizers are not able to solve these problems. Advanced control theories seem appropriate to design more powerful power system stabilizers.

Two power system stabilizers were developed based on robust control theory and adaptive control theory. The effectiveness of both stabilizers was evaluated as objectively as possible. The proposed control approaches were evaluated on a basis of a theoretical analysis and numerical simulations. The sliding mode stabilizer and direct adaptive stabilizer have the following advantages in comparison to conventional linear stabilizers:

• The proofs of the stability of the entire closed-loop system exist for both controllers presented.

• Both controllers require minimal preknowledge of the controlled plant structure and parameters.

• Both controllers have an uncomplicated tuning procedure.

- Both controllers do not require the measurement of the additional control plant variables.

- Both controllers are easy to implement (low computing demand and low sampling frequency).

- Both controllers damp oscillations in the entire operating range and assure stability.

- Both controllers do not calculate high output amplitudes and are insensitive to the actuator's saturations.

The comparison of the developed novel power system stabilizers shows the significant advantage of the modern concepts in all the considered ranges of the operation. Due to the actuality and importance of the issues tackled, the development of more effective power system stabilizers is inevitable. It is our estimation that the intensity of research in this field will increase in the future. In our evaluation, the robust and adaptive controls emerged as the most prospective concepts for implementation in power system stabilizers.

Author details

Jožef Ritonja
Faculty of Electrical Engineering and Computer Science, University of Maribor, Maribor, Slovenia

*Address all correspondence to: jozef.ritonja@um.si

IntechOpen

References

[1] International Energy [Internet]. 2020. Available from: https://www.iea.org/data-and-statistics?country=WORLD&fuel=Energy%20supply&indicator =Electricity%20generation%20by%20source [Accessed: January 19, 2020]

[2] Ritonja J. Adaptive stabilization for generator excitation system. COMPEL. 2011;**30**(3):1092-1108. DOI: 10.1108/03321641111111022

[3] Boldea I. Synchronous Generators. Boca Raton: Taylor & Francis Group; 2016

[4] Anderson PM, Fouad AA. Power System Control and Stability. Ames, Iowa: The Iowa State University Press; 1977

[5] Ritonja J, Petrun M, Černelič J, Brezovnik R, Polajžer B. Analysis and applicability of Heffron-Phillips model. Elektronika ir Elektrotechnika [Print ed.]. 2016;**22**(4):3-10. DOI: 10.5755/j01.eie.22.4.15905. Ilustr. ISSN: 1392-1215

[6] Kundur P. Power System Stability and Control. New York: McGraw-Hill, Inc.; 1994

[7] Heffron WG, Phillips RA. Effect of a modern amplidyne voltage regulator on underexcited operation of large turbine generators. AIEE Transactions. 1952;**71**: 692-697

[8] Bergen AR, Vittal V. Power Systems Analysis. Upper Saddle River, New Jersey: Prentice-Hall Inc.; 2000

[9] Demello FP, Concordia C. Concepts of synchronous machine stability as affected by excitation control. IEEE Tran. Power Appar. Syst. 1969;**88**(4):316-329

[10] Machowsky J, Bialek JW, Bumby JR. Power System Dynamics, Stability and Control. West Sussex, United Kingdom: John Wiley and Sons, Ltd.; 2008

[11] IEEE Std. IEEE recommended practice for excitation system models for power system stability studies. In: IEEE Std 421.5–2005, IEEE Power Engineering Society by Energy Development and Power Generation Committee; 21 April 2006

[12] Ritonja J, Dušak M. Analysis of the Slovenian Power System Stabilizers. Journal of Electrical Engineering and Computer Science. Ljubljana: Electrotechnical Society of Slovenia; 2014

[13] Utkin VI. Sliding mode control design principles and application to electric drives. IEEE Transactions on Industrial Electronics. 1993;**40**(1):23-36

[14] Bartolini G, Fridman L, Pisano A, Usai E. Modern Sliding Mode Control Theory. New York: Springer Verlag; 2008

[15] Slotine JJE, Li W. Applied Nonlinear Control. Englewood Cliffs, New Jersey: Prentice Hall Inc.; 1991

[16] Landau YD. Adaptive Control. New York: Marcel Dekker Inc.; 1979

[17] Eichmann A, Kohler A, Malik O P, Taborda J. A prototype self-tuning adaptive power system stabilizer for damping of active power swings. In: Power Engineering Society Proceedings of the Summer Meeting in Seattle, WA, Vol. 1. IEEE; 2000. pp. 122-126

[18] Ritonja J, Dolinar D, Grčar B. Simple adaptive control for a power-system stabiliser. In: IEEE Proceedings Control Theory and Applications [Print ed.]; 2000. pp. 373-380

[19] Kaufman H, Bar-Khana I, Sobel K. Direct Adaptive Control Algorithms. New York: Springer Verlag; 1993

[20] Šabanovic A. Variable structure systems with sliding modes in motion control—A survey. IEEE Transactions on Industrial Informatics. 2011;7(2):212-223